THE HIGHLY ECCENTRIC DELTA SCORPII BINARY SYSTEM

Ashley Ames

A thesis submitted in partial fulfillment of
the requirements for the degree of
Master of Science

Department of Physics

Central Michigan University
Mount Pleasant, Michigan
July 2011

Accepted by the Faculty of the College of Graduate Studies,

Central Michigan University, in partial fulfillment of

the requirements for the master's degree

Thesis Committee:

Tycner — Committee Chair

Marco Fornari — Faculty Member

Glen Williams — Faculty Member

Date: 07/12/2011

Dean
College of Graduate Studies

Date: 10/24/11

Committee:

Christopher Tycner, Ph.D., Chair

Marco Fornari, Ph.D.

Glen Williams, Ph.D.

ACKNOWLEDGEMENTS

I wish to thank the members of the thesis committee: Dr. Christopher Tycner, Dr. Marco Fornari, and Dr. Glen Williams. All of these faculty members have contributed to making this thesis what it has become. In addition, I wish to thank the entire physics department for all of their help and support through the duration of this project. I would also like to thank the members of the NPOI group who have taken time to answer questions and allow me to use their data. Finally, I wish to acknowledge the support of Central Michigan University in producing this work.

ABSTRACT

THE HIGHLY ECCENTRIC δ SCORPII BINARY SYSTEM

by Ashley Ames

In anticipation of the possible collision between a circumstellar disk and the secondary star in the highly eccentric binary system δ Scorpii, high angular resolution optical interferometric observations have been obtained and used to revise the binary parameters. The Navy Prototype Optical Interferometer was used to spatially resolve the binary components and circumstellar disk size in 2000 and over a period between 2005 and 2011. The interferometric observations are used to obtain the angular separations and orientations of the two stellar components at all epochs for which data have been obtained, including 2005 and 2006, which previous studies have stated there was some uncertainty as to if the signature of the binary can be clearly detected. The observations also specify the disk size in the Hα-emitting region by fitting a Gaussian to the data. The results of this study represent the most complete and accurate coverage of the binary orbit of this system to date and allow for the revised timing of the upcoming periastron passage that will occur in 2011 to be obtained. In addition, the disk size associated with the primary star is determined as a function of time. The most recent result for the disk size in 2011 was 2.4 ± 0.2 mas. These results imply that there will not be a direct collision between the disk and the secondary star during the upcoming periastron passage, but a significant gravitational interaction can be expected.

TABLE OF CONTENTS

LIST OF TABLES vi

LIST OF FIGURES vii

CHAPTER

I. INTRODUCTION 1

II. BINARY STARS 5
2.1 Kepler's Laws 5
2.2 Orbital Parameters 9
2.3 Previous Spectroscopic Results 19

III. INTERFEROMETRIC OBSERVATIONS 21
3.1 Principles of Long-Baseline Interferometry 2
3.2 Navy Prototype Optical Interferometer (NPOI) 26
3.2.1 Reduction Procedures 26
3.2.2 Calibration 30
3.3 Observational Results 32
3.3.1 Refined Orbit 32
3.3.2 Errors on ρ_{min} 37

IV. CIRCUMSTELLAR DISK 39
4.1 Background 39
4.1.1 The Cirumstellar Diskof δ Sco 42
4.2 Determining Disk Characteristics 45
4.3 Disk Parameters 60

V. CONCLUSIONS 64
5.1 Binary Orbit 64
5.2 CS Disk 65
5.3 Future Work 66

APPENDICES 67

BIBLIOGRAPHY 122

LIST OF TABLES

TABLE PAGE

3.1 The orbital elements for δ Sco.....34

4.1 The Hα equivalent widths and the corresponding c_p value.....53

4.2 Disk size.....62

LIST OF FIGURES

FIGURE PAGE

2.1 A graphical representation of an elliptical orbit in the true plane being projected onto the plane of the sky (figure based on Fig. 7 of Heintz, 1978, p.32).....10

2.2 A graphical representation of an elliptical orbit with the auxiliary circle. This shows how the true anomaly and eccentric anomaly as well as other elliptical can be derived (figure based on Fig. 8 from Heintz, 1978, p. 35) 15

3.1 A scan of δ Sco showing the binary signature in the form of a modified cosine. Channel 10 represents the Hα channel were the disk signature is present 25

3.2 An idealized interferometer schematic (figure from Fig. 2.1 in Boden, 2000, p. 11) 28

3.3 Example of NAT counts for an input beam (i.e., a siderostat). The red dots are the flagged data points. The points inside the black box represent a count drop which could be explained by the target being blocked by a cloud or loss of tracking 29

3.4 Radial velocities of the system, plotted again the epoch, from Miroshnichenko et al. (2001). Included are the residual velocities determining how good a fit the orbital parameters are to the data 33

3.5 The periastron passage marked with an X. The predicted positions of the secondary are plotted on the orbit, 10 days (triangle), 30 days (diamond), and 60 days (box), before and after the periastron passage. Locations of the secondary along the newly revised orbit from previous periastron results are shown (pluses) 35

3.6 Top: binary orbits based on orbital parameters obtained from this paper (solid, blue), Tango et al. (2009) (orange, dashed), Mason et al. (2009) (light blue), and Miroshichenko et al. (2001) (green). The filled, black circles are the astrometric results. The error ellipses are plotted over the data points (red). The locations of the primary is marked with an X. Bottom panel: The east-west (squares) and north-south (crosses) represent the O-C vectors as a function of P.A. of the secondary.....36

3.7 Histogram of solutions obtained for the apparent separation of the secondary and primary star during the periastron passage, based on 300,000 synethic data sets sets 38

4.1 A schematic representation of the binary system along the North axis 47

4.2 A schematic representation of the visibilities of the binary system in the complex plane.....50

4.3 A schematic representation of the binary system where $V_{H\alpha}$ is parallel to V_1.....54

4.4 The total phase, ϕ, is plotted in frame 1. The phase contribution from V_1 is plotted in frame 2. Frame 3 contains the resulting phase subtraction β. The phase is plotted as a function of wavelength, with a baseline length of 40 m, an apparent separation of 192.92 mas and a Δm of 2.2 (Tango et al., 2009).....56

4.5 Panel (a): A comparison of how the Δm affects the β angle. Δm includes 1.0, 2.2, and 3.0 respectively, with a baseline of 40 m and apparent separation of 192.92 mas. Panel (b): A comparison of how the projected separation affects the frequency of the β angle. The separation includes 20, 100, and 192.92 mas respectively with a baseline of 40 m and Δm of 2.2 (Tango et al., 2009).....57

4.6 Disk size fitted, to 2005 data, with a Gaussian. Each panel represents separate synthetic stars added to the data set with different c_p values. In this case, the most realistic synthetic star addition is the $c_p = 0.8269$ because that should be how much the star actually contributes to the system.....61

4.7 Disk size plotted as a function of time. The averaged values with the errors are from Table 4.2 63

CHAPTER I

INTRODUCTION

δ Scorpii (HD 143275, HR 5953, FK5594, δ Sco) is a well known highly eccentric binary system with a primary star that possesses a circumstellar disk (these type of stars are of the spectral type B with prominent emission lines of hydrogen, Be stars). This particular system has been observationally investigated using interferometry, spectroscopy, and photometry. The main interest in this system is to determine whether the primary star's circumstellar disk and the secondary come close enough during the upcoming periastron passage expected in 2011 for there to be a collision or interaction between the two. There have been many attempts at refining the binary orbit using speckle interferometry. Several studies have been done to revise the binary parameters, which in turn estimate the date of the upcoming periastron passage. Hartkopf et al. (1996) determined that previous findings of Bedding (1993) had underestimated the eccentricity of the orbit. It was calculated that an eccentricity of 0.92 seemed to fit the orbit well, but they speculate that a coverage of the orbit (especially during the periastron passage in 2001) was needed to define the unresolved portion of the orbit to obtain an accurate measurement of the masses and distance.

Miroshnichenko et al. (2001) not only obtained the radial velocities of the system, but observed that the disk-star system fluctuates in intensity. Observations showed that the primary was marginally brighter in 2000. After it dipped in brightness in 2000, it remained

stable at 1.89 apparent magnitude. The increase in brightness can be explained due to the disk gaining more material from the primary star. Since the secondary was very close to the primary during the last periastron passage, it limited the disk's ability to grow. After periastron passage, the disk was able to grow freely again which implies that the periastron passage might be connected to the mass loss process of the primary star (Miroshnichenko et al., 2001). Interferometric data obtained from this project will be analyzed to determine if the disk has changed in size between 2005 and 2011.

There have been some discrepancies whether the secondary can be seen throughout the entire orbit. Observations of the δ Sco system were made with the Sydney University Stellar Interferometer (SUSI) between 1999 and 2007 (Tango et al., 2009). Based on these observations, Tango et al. (2009) reports that in 2006 all they could resolve was the primary star implying it being the dominant contribution to the light and no signature of binarity was detected. In this study, we will show that the binary signature is detected not only in 2006, but at all other epochs covered by our interferometric observations obtained in 2000 and from 2005 to 2011.

The disk parameters associated with the primary star is an important feature of this system. Models have been created to represent the disk around the primary. Carciofi et al. (2006) determined that the system was a non-eclipsing binary with a B0-type primary and a secondary being 1.5 mag optically fainter. It was concluded that the disk was geometrically

thin in the vertical direction, as well as nonisothermal and completely ionized. For their model, only 10 percent of the stellar flux can be blocked by the disk and they concluded that the geometry of the system has to change over time to explain the stellar flux variations. Carciofi et al. (2006) concluded that their static model could not explain the fading of the light with anti-correlation in the Balmer series Hα line strength. Because the Hα line strength has increased, it was concluded that the disk was growing in size. Interferometry combined with spectroscopic data can provide more insight into the structure and size of the disk as well as how it has fluctuated over several years.

Photometric observations were obtained for δ Sco in the IR portion of the spectrum by Halonen et al. (2008). A model was created for the disk which describes its radial density distribution. The model assumed that the density decreases as an inverse power law. Halonen et al. (2008) determined that the density falls off as $r^{-3.5}$. It was also concluded that the disk has a Keplerian rotation and that the best model was a disk at an inclination angle of 20°, with respect to the sky, with an evacuated ring in the center (Halonen et al., 2008). To date, no interferometric data has been obtained to support an evacuated ring in the center of the circumstellar disk. The observations presented in this study can be used to test whether a ring like structure has formed within the disk.

The purpose of this project is to refine the binary parameters of the δ Sco system and resolve the circumstellar disk around the primary star. Since there is a possibility of

the secondary star colliding or interacting with the disk around the primary star, the orbital parameters need to be highly accurate such that the periastron passage can be predicted to within a few days. The period of the orbit along with the date of the periastron passage is one of the most important aspects of refining the orbit, especially if observations are to be properly scheduled during the periastron passage of 2011. Due to the high eccentricity of the δ Sco system, the secondary star is moving very quickly near and during the periastron passage, due to Kepler's second law, and finding the precise timing of the passage is crucial for any observational measurements to be made on the system. Resolving the disk is necessary because even if the secondary does come very close to the primary, the physical extent of the disk is what will ultimately determine whether the secondary will collide or interact with the circumstellar disk around the primary.

CHAPTER II

BINARY STARS

A binary system consists of two stars orbiting around a common center of mass. If the primary star is much more massive then the secondary, then the center of mass will be closer to the center of the primary star. In this case, the secondary will appear to orbit the primary star as seen in the δ Sco system.

2.1 Kepler's Laws

The motion of stars and planets follow Kepler's three laws. The first law states that the orbit of a binary system is an ellipse with the primary star at one of the foci. The second law states that the radial vector sweeps out equal areas in equal intervals of time. The second law is a general theorem for central force motion. The second law is derived using the Lagrangian in polar coordinates

$$L = T - V = 1/2m(\dot{r}^2 + r^2\dot{\theta}^2) - V(r), \tag{2.1}$$

where $V(r)$ is the potential and a function of only r because force of gravity is a radial (central) force. In this case, θ is a cyclic coordinate since

$$\frac{\partial L}{\partial \theta} = 0 \tag{2.2}$$

and

$$\frac{\partial L}{\partial \dot{\theta}} = p_\theta = \text{constant} = l \tag{2.3}$$

where l is a constant of angular momentum. From equations 2.1 and 2.3 we get

$$p_\theta = mr^2\dot{\theta} \tag{2.4}$$

or

$$\frac{p_\theta}{2m} = \frac{1}{2}r^2\dot{\theta} = \frac{l}{2m}. \tag{2.5}$$

This implies that the momentum, p_θ, is a conserved quantity and that the coordinate θ is cyclic and conserved. The factor of $\frac{1}{2}$ is inserted in the above equation because it is the area that is swept out by the radius per unit time. The differential area that is swept out is

$$dA = \frac{1}{2}r\,(r d\theta) \tag{2.6}$$

hence,

$$\dot{A} = \frac{1}{2}r^2\dot{\theta}. \tag{2.7}$$

Equation 2.7 illustrates that the differential area is swept out at a constant rate (Kepler's 2nd law). This particular law is very important in the δ Sco system since the orbit

is highly elliptical. As the secondary approaches the primary star, it is moving quickly and as Kepler's second law illustrates, it must cover the same area as in other parts of the orbit. Since the area swept out during the closest approach is the same that is swept out at a time of large separation, this states the secondary will move faster as it approaches the primary.

The third law states that the square of the orbital period is proportional to the cube of the semi-major axis. The third law is restricted to the inverse square law of force. Kepler's third law can be derived directly from properties of an ellipse and from the second law. Using equation 2.5 and 2.7, the second law can be written as (Goldstein, 1980, pp. 98–100 for full derivation)

$$\dot{A} = \frac{1}{2} r^2 \dot{\theta} = \frac{l}{2m}. \tag{2.8}$$

The area of the orbit, A, can be found by integrating over a period, τ

$$\int_0^\tau \frac{dA}{dt} dt = A|_0^\tau = \frac{l\tau}{2m}. \tag{2.9}$$

Since the area of an ellipse is

$$A = \pi ab. \tag{2.10}$$

We can substitute equation 2.10 into equation 2.9 and using the following expressions for ellipses (eq. 3-62 in Goldstein, 1980, p. 97)

$$b = a\sqrt{1-e^2}, \tag{2.11}$$

with

$$e = \sqrt{1-\frac{l^2}{mka}} \tag{2.12}$$

where a is the semi-major axis, b is the semi-minor axis, $k = Gm_1m_2$, and e is the eccentricity of the conic section. If $e < 1$ then that implies an elliptical orbit. By replacing e in equation 2.11 with equation 2.12, the semi-minor axis then becomes

$$b = a^{\frac{1}{2}}\sqrt{\frac{l^2}{mk}}. \tag{2.13}$$

Therefore, the period from equation 2.9 reduces to

$$\tau = \frac{2m}{l}\pi a^{\frac{3}{2}}\sqrt{\frac{l^2}{mk}} = 2\pi a^{\frac{3}{2}}\sqrt{\frac{m}{k}}. \tag{2.14}$$

However, to account for the two-body problem, m must be replaced by the reduced mass of the system

$$\mu = \frac{m_1m_2}{m_1+m_2} \tag{2.15}$$

where m_1, m_2 refer to the mass of each object and τ^2 can be written as

$$\tau^2 = \frac{4\pi^2 a^3}{G(m_1 + m_2)}. \tag{2.16}$$

Kepler's third law states that the square of the period is proportional to the cube of the semi-major axis. Any two body problem, including binary stars, are governed by Kepler's three laws.

2.2 Orbital Parameters

Any binary system is classified by specific characteristics of the system. Among the classifications, δ Sco is known as both a visual and a spectroscopic binary. Visual binaries consist of two stars that have a high enough angular separation that the stars can be resolved by a telescope. The brightness ratio of the stars affects whether the stars can be resolved. For visual binaries, there are seven orbital elements that relate the motion of the companion with respect to the primary star.

In the case of a visual binary, the observed shape of the orbit does not represent the actual physical orbit since the orbit is typically seen at an arbitrary angle. In other words, the observed orbit represents the projected orbit onto the celestial sphere (i.e., the plane of the sky). This will change the way the orbit is seen depending on the particular angle with respect to the observer. If the orbit is circular, the projected orbit will look more elliptical

depending on how great the inclination angle flattened out the true orbit. Typically, the plane of the orbit is not perpendicular to our line of sight so the system will have a true orbit and a projected orbit. Four elements define the properties of the true orbit: the period (P) of the secondary (the time it takes the secondary to complete one revolution) measured in years, the epoch (T) of passage of the secondary through the periastron, which is the closest approach of the secondary to the primary star, the semi-major axis (a) of the true orbit (given in arc-seconds), and the eccentricity (e) of the orbit.

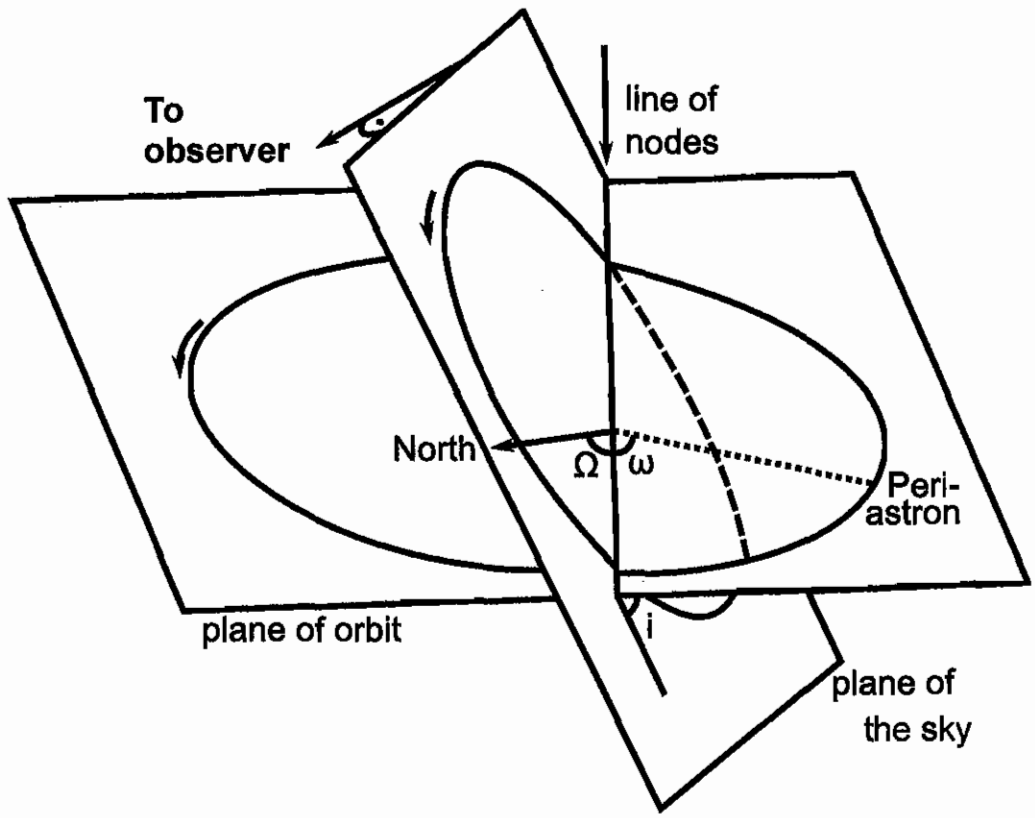

Figure 2.1. A graphical representation of an elliptical orbit in the true plane being projected onto the plane of the sky (figure based on Fig. 7 of Heintz, 1978, p. 32).

Three of the seven orbital elements depend on the projections of the true orbit onto the plane of the sky (Figure 2.1). The line of nodes is the intersection between the tangential plane of projection and the true orbital plane. There are two different nodes which differ by 180°. The node which has the orbital motion directed away from the observer is called the ascending node. The ascending node is only defined by the radial velocities of the system and not the positional data. The ascending node is the node where the secondary passes away from the observer and the descending node is the node where it moves towards the observer. The projected orbit is at a tilt angle, i, with respect to the plane of the sky and is known as the inclination angle. The inclination angle can range from 0° to 180°. The motion of the secondary is in the direction of the increasing position angle if $i < 90°$. If $i > 90°$ there is retrograde motion and if $i = 90°$ then the motion is projected directly onto the line of nodes. The inclination angle requires careful measurements of the apparent orbit in order to deduce the true orbit of the system. Sometimes this angle cannot be measured and remains unknown. The angle of the true orbital plane to the line of nodes and periastron passage (ω) is measured in the direction of motion from 0° to 360°. This parameter describes how the true orbit is oriented in the plane of the sky.

To obtain rectangular or spherical coordinates from the orbital elements the Thiele-Innes elements are used (from eq. 6 and 7 in Heintz, 1978, p. 33), which have the form

$$A = a(\cos\omega\cos\Omega - \sin\omega\sin\Omega\cos i) \tag{2.17}$$

$$B = a(\cos\omega\sin\Omega + \sin\omega\cos\Omega\cos i) \tag{2.18}$$

$$F = a(-\sin\omega\cos\Omega - \cos\omega\sin\Omega\cos i) \tag{2.19}$$

$$G = a(-\sin\omega\sin\Omega + \cos\omega\cos\Omega\cos i). \tag{2.20}$$

To obtain the radial coordinate the following two expressions are also used

$$C = a\sin\omega\sin i, \tag{2.21}$$

and

$$H = a\cos\omega\sin i. \tag{2.22}$$

These constants are derived using Euler angles. The orientation of the apparent orbit is achieved by using three elemental rotations around a single axis. The first rotation consists of rotating the true orbit from "North" by an angle Ω, which defines the line of nodes, and

can be written in a matrix form as

$$\mathbf{M}_{\Omega} = \begin{pmatrix} \cos\Omega & \sin\Omega & 0 \\ -\sin\Omega & \cos\Omega & 0 \\ 0 & 0 & 1 \end{pmatrix}. \tag{2.23}$$

This rotation is occurring around the z-axis, the axis that is perpendicular to the true orbit, which results in the entry, in the third row and column to be unity. The next rotation is described by ω which determines the orientation of the periastron. Again the z-axis will be constant, and the matrix has the form

$$\mathbf{M}_{\omega} = \begin{pmatrix} \cos\omega & \sin\omega & 0 \\ -\sin\omega & \cos\omega & 0 \\ 0 & 0 & 1 \end{pmatrix}. \tag{2.24}$$

The inclination angle is determined by rotating the coordinate system around the x-axis, along the line of nodes. This determines how the true orbit is projected onto the celestial

sphere to give the apparent orbit

$$\mathbf{M_i} = \begin{pmatrix} 1 & 0 & 0 \\ 0 & \cos i & \sin i \\ 0 & -\sin i & \cos i \end{pmatrix}. \tag{2.25}$$

To obtain the Thiele-Innes constants all three matrices must be multiplied together with a factor of a (the semi-major axis) $\mathbf{M}_\omega \mathbf{M}_i \mathbf{M}_\Omega$. Using equations 2.17, 2.18, 2.19, 2.20, 2.21 and 2.22 gives the following matrix

$$\mathbf{M} = a \begin{pmatrix} A & B & C \\ F & G & H \\ \sin\Omega\sin i & -\cos\Omega\sin i & \cos i \end{pmatrix}. \tag{2.26}$$

The apparent orbit uses rectangular coordinates defined as x and y. The true orbit uses normalized rectangular coordinates defined as X and Y. To find the normalized rectangular coordinates, an auxiliary circle is needed. An auxiliary circle is a circle whose center is the same as the ellipse and radius is equal to the semi-major axis of the ellipse (Figure 2.2). This relates the normalized rectangular coordinates to the true anomaly and eccentric anomaly. The true anomaly is the angle between the periastron and the position of the celestial object as seen from the main focus (where the primary is located) of the

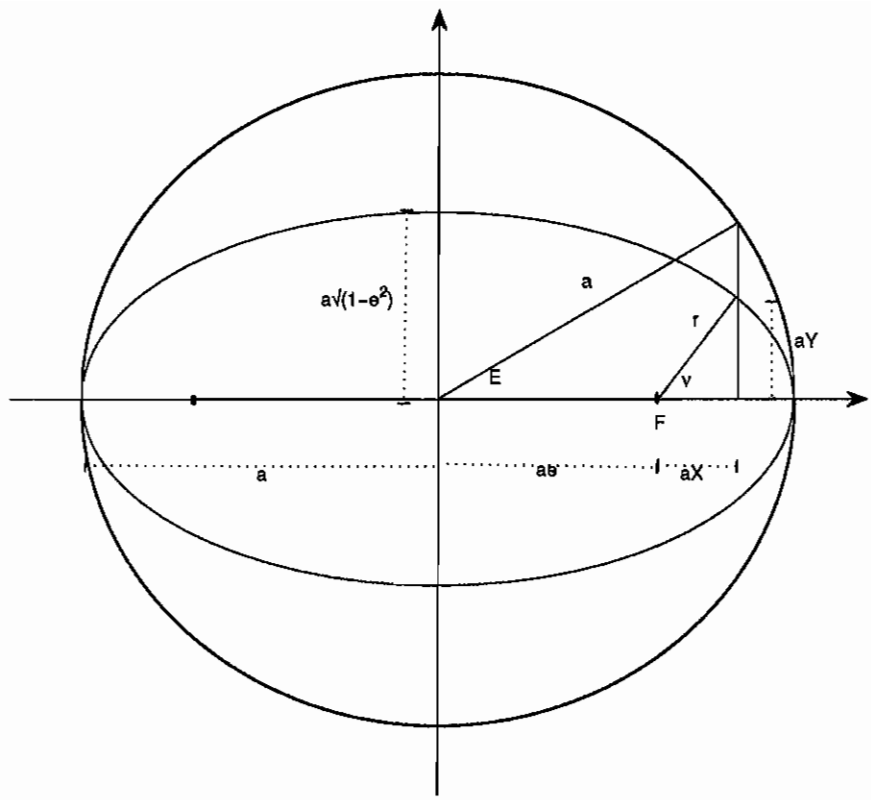

Figure 2.2. A graphical representation of an elliptical orbit with the auxiliary circle. This shows how the true anomaly and eccentric anomaly as well as other elliptical properties can be derived (figure based on Fig. 8 from Heintz, 1978, p. 35).

ellipse and the eccentric anomaly is the angle measured at the center of the circle, from the periastron to a point on the circle which is found from a line perpendicular to the major axis that goes through a location in the orbit (Figure 2.2). The two angles for the true and eccentric anomaly are denoted by ν and E, respectively. Following simple geometry, X can be found where

$$\cos E = \frac{a(e+X)}{a}, \tag{2.27}$$

or

$$X = \cos E - e, \tag{2.28}$$

where e is the eccentricity. To find Y, the true anomaly must be used where

$$\cos \nu = \frac{aX}{r}, \tag{2.29}$$

and

$$\sin \nu = \frac{aY}{r}. \tag{2.30}$$

The radial distance of the true orbit is defined by (eq. 3-64 in Goldstein (1980), p. 98 and eq. 11 in Heintz (1978), p. 34)

$$r = \frac{a(1-e^2)}{1+e\cos\nu}. \tag{2.31}$$

Replacing r and X in equation 2.29 using equations 2.31 and 2.28 results in the following equation

$$\cos \nu = \frac{\cos E - e}{1 - e\cos E} = \frac{X}{r/a}, \tag{2.32}$$

where r in terms of the eccentric anomaly can be expressed as

$$r = a(1 - e\cos E), \tag{2.33}$$

and X can be written as

$$X = \cos E - e, \tag{2.34}$$

which is in agreement with equation 2.28. Using the identity of

$$\sin\nu = \sqrt{1 - \cos^2\nu}, \tag{2.35}$$

equation 2.35 can be written as

$$\sin\nu = \frac{\sqrt{1-e^2}\sin E}{1 - e\cos E}. \tag{2.36}$$

To find Y, the expression for tangent can be used

$$\tan\nu = \frac{Y}{X} = \frac{\sqrt{1-e^2}\sin E}{\cos E - e}, \tag{2.37}$$

which implies

$$Y = \sqrt{1-e^2}\sin E. \tag{2.38}$$

The relation between the apparent orbit in rectangular coordinates and the orbit as described by X and Y is described by (eq. in 16 in Heintz, 1978, p. 34)

$$x = AX + FY, \tag{2.39}$$

$$y = BX + GY, \tag{2.40}$$

where X and Y are from equations 2.28 and 2.38 and A, B, F, G, X are from equations 2.17-2.20 and 2.26. These terms are used to plot the apparent rectangular coordinates for an ellipse using all the elements of an elliptical orbit.

Although the δ Sco system has been resolved visually using interferometric methods (Hartkopf et al., 1996; Mason et al., 2009; Tango et al., 2009), the orbital parameters are not as accurate as needed for predicting accurately the timing of the upcoming periastron passage in 2011. Finding the date of the minimum separation between the secondary and primary star is essential if astronomers wish to study this system in more detail. The interaction between the two stars will occur during the periastron passage and the date of the periastron passage must be found to within a few days. The goal for this project is to revise the orbital parameters so that the timing of the periastron passage will be known within uncertainties of no more than a day or two.

2.3 Previous Spectroscopic Results

Spectroscopic binary systems are observed by obtaining the system's spectrum. Typically when observing the system, the motion of the stars around the center of mass will result in a Doppler shift of both stars which will be apparent in the spectrum of the binary. If the spectral lines from both stars are visible, then the spectral lines will shift from a higher to lower frequency periodically and the system is called a double-lined spectroscopic binary. The two stars will shift in opposite directions, meaning when star A is moving toward the observed and the spectrum is shifted to a higher frequency, star B will move away from the observer and the spectrum will be shifted to a lower frequency. If the spectrum from only one of the components can be observed, due to the spectral lines being much stronger from one of the stars, then the binary is known as a single-lined binary system. The orbit of the binary is determined by making several observations to obtain the radial velocity of the stars. Radial velocity is the speed at which the stars are moving towards or away from the observer. If the radial velocity is positive, the object is receding and has a redshift. If the radial velocity is negative, the object is approaching and has a blueshift. Radial velocities of the stars can be used to find the masses of the stars as long as the parallax is known and orbital elements such as the semi-major axis and eccentricity are known. Typically, observations obtained of the stars are plotted against time and from the

curve a period is determined. If the orbit is elliptical, the shape will depend on the inclination angle and the eccentricity of the orbit. For a single-lined spectroscopic binary with a high eccentricity, the shape of the radial velocity curve will have an absolute minimum approximately where the periastron passage is located.

Since δ Sco has properties of both a visual and spectroscopic binary, observations have been taken that visually resolve the system. Spectroscopic observations were obtained from Miroshnichenko et al. (2001, 2003). It has been determined that the system is a single-lined spectroscopic binary due to the relatively high flux ratio between the two components. Measurements of the system's radial velocity has produced a highly accurate measurement of the last periastron passage that occurred in 2000 (Miroshnichenko et al., 2001). From this data, the radial velocities of the system have been well defined along with the mass estimates.

CHAPTER III

INTERFEROMETRIC OBSERVATIONS

3.1 Principles of Long-Baseline Interferometry

Interferometry consists of two or more telescopes along a line, called a baseline, combining light in a constructive and destructive manner to achieve higher angular resolution. The data we have obtained for the purpose of this study were obtained using the Navy Prototype Optical Interferometer, located near Flagstaff, Arizona. NPOI consists of 6 stations that are used for imaging. The telescopes can be moved to form baselines of lengths ranging from 16 to 80 meters. For a perfect telescope without atmospheric turbulence and optical imperfections, the ideal angular resolution that can be obtained is given by the Rayleigh criterion

$$\sin\theta = 1.22\frac{\lambda}{D}, \tag{3.1}$$

where θ is the angular resolution of the telescope in radians, λ is the wavelength of the light, and D is the diameter of the aperture. However, it is very expensive to build a telescope of an aperture size of 50 meters or more, but the same resolution is easily obtained from an interferometer. The angular resolution obtained from the length of the baseline is the same as if a telescope had an aperture of the same size.

The light beams obtained from the telescopes in an interferometer will interfere constructively or destructively to create a fringe. The baseline is projected onto the sky

and determines the achievable resolution. The baseline coverage on the sky is measured through spatial frequencies, u and v which have units of fringe cycles per radian on the sky and is given by

$$u \equiv \frac{B_x}{\lambda}, \tag{3.2}$$

and

$$v \equiv \frac{B_y}{\lambda}, \tag{3.3}$$

where B is the baseline length. Typically, u and v are defined to correspond to directions of right ascension and declination on the sky, respectively. Interferometers measure the amplitude of the complex visibility function which describes the contrast and the phase of a fringe pattern. Optical interferometers usually measure the normalized fringe visibility or squared visibility, which is the fringe power obtained relative to the total power collected from the source. Originally Michelson defined the visibility of the fringes to be the contrast between the light and dark areas ($P_{\max}$ and $P_{\min}$ respectively). This determined the Michelson fringe visibility (Boden, 2000, p. 19)

$$\mathrm{v}_M \equiv \frac{P_{\max} - P_{\min}}{P_{\max} + P_{\min}}. \tag{3.4}$$

Equation 3.4 is dimensionless and contained in the interval [0,1]. As the observed source becomes more resolved the fringe "washes out" and $P_{\max} = P_{\min}$ thus $\mathrm{v}_M = 0$. The visibility

measured determines the coherent response of the interferometer due to the astronomical source (eq. 2.15 in Boden, 2000, p. 17) and can be expressed in the following form

$$V(u,v) = \int \mathrm{d}\alpha \mathrm{d}\beta A(\alpha,\beta) F(\alpha,\beta) e^{-2\pi i(\alpha u + \beta v)}, \tag{3.5}$$

which is a complex quantity with dimensions of power (due to the product of the effective cross-sectional area, A, and spectral intensity, F). In this case, the visibility of the fringe can be used to obtain the source brightness distribution on the sky, via a Fourier transform of the form (eq. 2.17 in Boden, 2000, p. 18)

$$F(\alpha,\beta) = \frac{\int \mathrm{d}u\mathrm{d}v \mathrm{V}(u,v) e^{2\pi i(\alpha u + \beta v)}}{A(\alpha,\beta)}. \tag{3.6}$$

An unresolved star can be approximated by a point source which can be represented as a delta function. The brightness distribution with respect to the source coordinates (α_0, β_0) follows

$$F_0 \delta(\alpha - \alpha_0)\delta(\beta - \beta_0). \tag{3.7}$$

Using equation 3.5, the visibility is obtained through a Fourier transform

$$V(u,v) = \int \mathrm{d}\alpha \mathrm{d}\beta A(\alpha,\beta) F_0 \delta(\alpha - \alpha_0)\delta(\beta - \beta_0) e^{-2\pi i(\alpha u + \beta v)} = P_0 e^{-2\pi i(\alpha_0 u + \beta_0 v)}, \tag{3.8}$$

where this is the total power times a phase factor (eq. 2.22 in Boden, 2000, p. 22). The normalized visibility is

$$\nu = e^{-2\pi i(\alpha_0 u + \beta_0 v)}, \tag{3.9}$$

which is in the interval [0,1] (eq. 2.23 in Boden, 2000, p. 22).

For multiple stellar systems the total received power of the system is the sum of the power from the visible sources

$$P_o = \sum_j P_j. \tag{3.10}$$

This is because the light from each star does not interfere constructively or destructively (photons from one star have no knowledge about another star). Normalized visibility becomes (eq. 2.30 in Boden, 2000, p. 26)

$$\nu = \frac{\sum_j P_j \nu_j}{\sum_j P_j}. \tag{3.11}$$

For a two component system the visibility becomes

$$\nu = \frac{P_1 \tilde{\nu}_1 + P_2 \tilde{\nu}_2}{P_1 + P_2}. \tag{3.12}$$

where $\tilde{\nu}_1$ and $\tilde{\nu}_2$ are complex quantities and are described by equation 3.9. Since optical long-baseline interferometers measure the ν^2 as opposed to the complex visibility, we are

interested in $v^2_{\rm binary}$ which is given by the squared modulus

$$v^2_{\rm binary} = v^*_{\rm binary}\, v_{\rm binary} \tag{3.13}$$

$$= \frac{v_1^2 + r^2\, v_2^2 + 2r\,|v_1|\,|v_2|\cos(\frac{2\pi\vec{B}\cdot\vec{s}_{\rm binary}}{\lambda})}{(1+r)^2}, \tag{3.14}$$

where $r \equiv P_2/P_1$, and P_2 and P_1 correspond to the power of the secondary and primary component, respectively, and (eq. 2.31 Boden, 2000, p. 26). The vectors $\vec{B}$ and $\vec{s}_{\rm binary}$ represent the vector separation between the baseline and binary components respectively. So when an interferometer measures the signature of a binary system, the signal will reflect a cosine function (Figure 3.1).

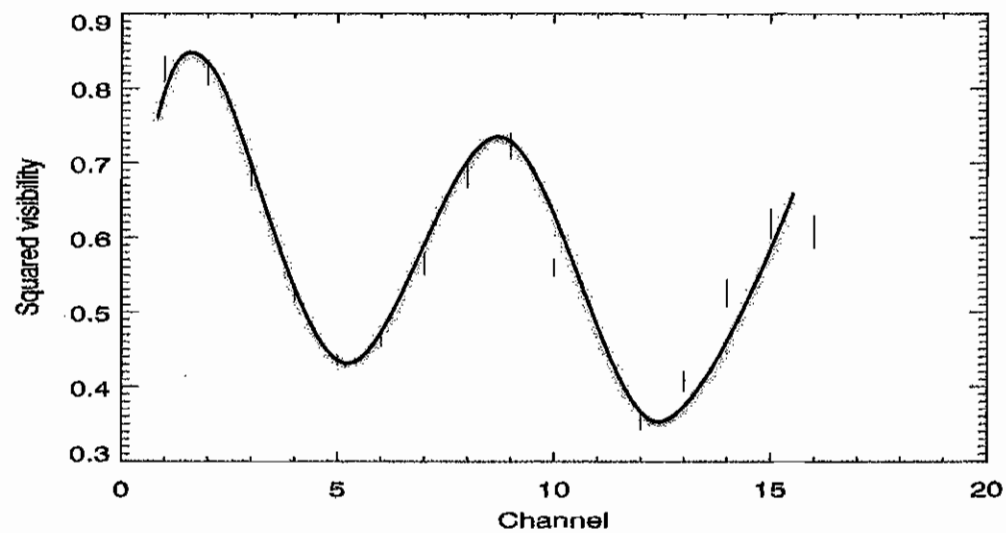

Figure 3.1. A scan of δ Sco showing the binary signature in the form of a modified cosine. Channel 10 represents the Hα channel where the disk signature is present.

The projection of the separation of the binary onto the baseline is given by $\vec{B} \cdot \vec{s}_{\text{binary}}$. The separation between the primary and secondary is given by $\vec{s}_{\text{binary}}$. Since the length of the baseline is known throughout the night, the $\vec{s}_{\text{binary}}$ can be measured. $\vec{s}_{\text{binary}}$ determines the frequency of the cosine which determines the separation, ρ and the position angle of separation, θ (measured East from North). The greater the separation between the two components, the higher the frequency of the cosine signature. As the separation decreases, the frequency of the cosine decreases as well. This is because the instrument cannot resolve the two sources separately and the stars are becoming a point source. Each scan obtained from NPOI is reduced to give astrometric measurements. These astrometric measurements contain information about the position of the secondary, on the sky, with respect to the primary star. Each scan from the night has the signature of the binary which is a cosine (equation 3.14 and Figure 3.1). From that cosine two parameters, ρ and θ, can be determined from the frequency. This in turn gives the position of the secondary along the orbit around the primary star.

3.2 The Navy Prototype Optical Interferometer (NPOI)

3.2.1 Reduction Procedures

Each observing night at NPOI produces a raw data file that contains all the fringe information on all sources observed. Each data file is downloaded, from the NPOI website,

in a compressed file format which is opened through a program called OYSTER. All reductions are done using the steps outlined in Hummel et al. (2003). The computer control system determines how to combine the light from the telescopes so that the light beams interfere constructively. However, during the first step of the reduction, it is necessary to remove the errors introduced by the computer control system. Even though two or more telescopes observe the same object, the wave-fronts may not be incident on the mirrors at the same time. The object is typically observed at some angle and thus the light may not travel the same distance (Figure 3.2). Since the light has to travel a further distance to the second telescope, the wavefront will reach the first telescope earlier. This means the wavefronts will be out of sync and the interference pattern will not be created (i.e., the light beams will simply add incoherently). Therefore, the extra paths (delays) must be introduced into the system to make up for the time and distance difference. The length is controlled by an automatic mirror on a cart that moves along in the Fast Delay Lines (FDLs), which are 18 m long vacuum tubes that are controlled by the computer. OYSTER automatically detects the error from the mirrors which is called the FDL delay residual. It also determines the amplitude of vibrations of the mirrors within the delay line as the cart moves along in the pipe (this is also known as delay jitter). If the signal is elevated it is an indication of the mirror moving too much within the pipe. These points are flagged and removed from the analysis.

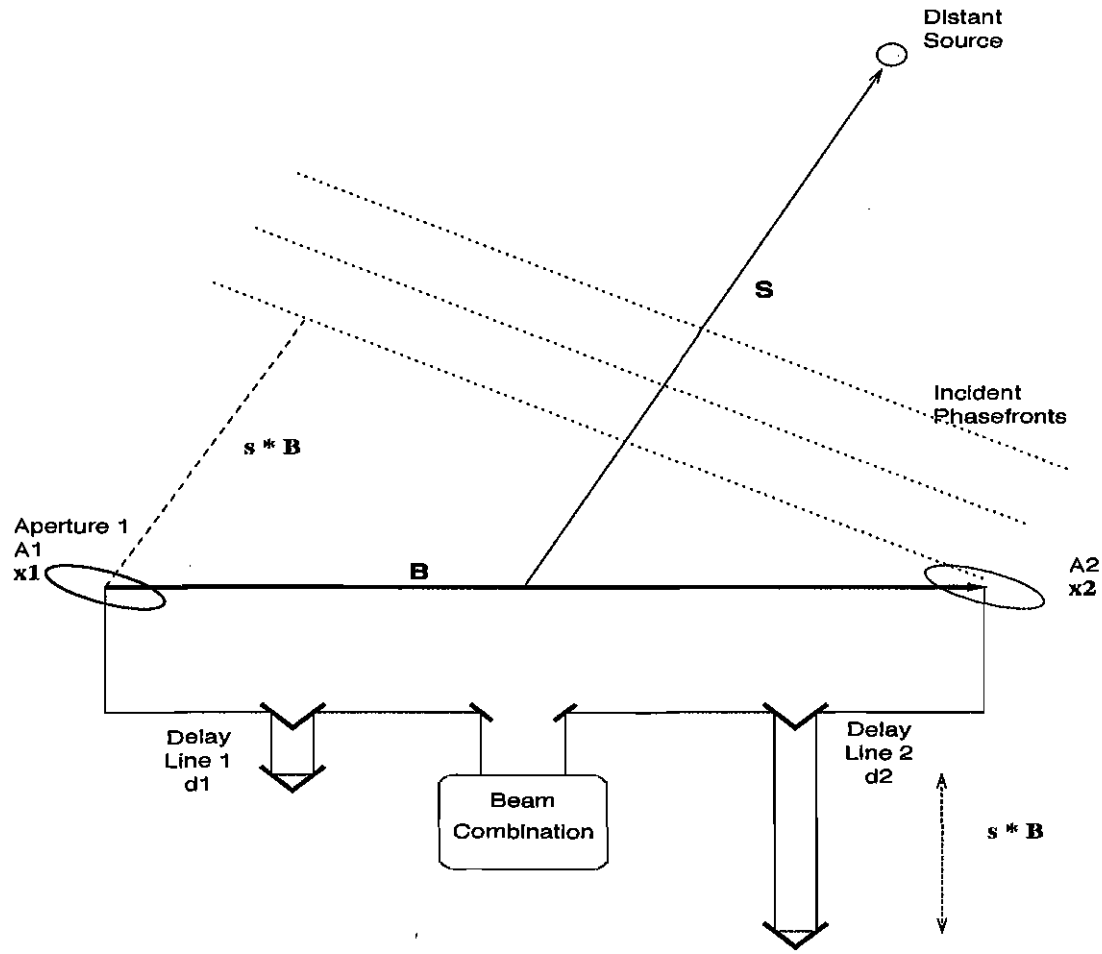

Figure 3.2. An idealized interferometer schematic (figure from Fig. 2.1 in Boden, 2000, p. 11).

The next step is done to account for atmospheric effects. When a wavefront is incident on the mirrors it has passed through atmosphere that can be quite turbulent. The light is incident on a mirror called a siderostat and reflected to the Narrow Angle Tracker (NAT) mirror which is similar to the secondary mirror on a telescope. In OYSTER, the NAT counts are recorded to determine how many photons were detected on the mirror before the light is reflected into the elevator can and sent to the beam combination system.

If there is a significant decrease in NAT counts, this is a possible result of a cloud covering the target. These scans are removed since something from the atmosphere has disturbed the signal (Figure 3.3).

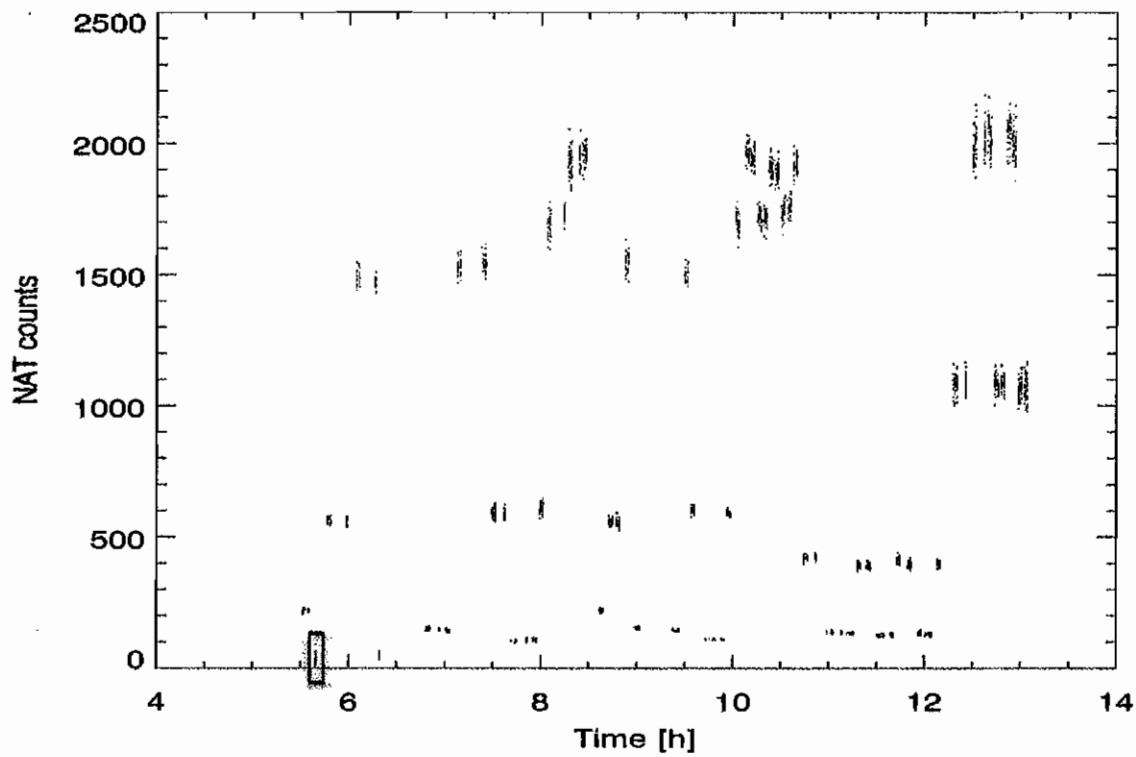

Figure 3.3. Example of NAT counts for an input beam (i.e., a siderostat). The red dots are the flagged data points. The points inside the black box represent a count drop which could be explained by the target being blocked by a cloud or loss of tracking.

Next the NAT jitter, which is similar to the delay jitter, measures how much the mirror has to move to keep the beam centered through the feed system and aligned into the beam combiner. The more the atmosphere is unstable, the more NAT mirror jitters. When the mirror jitters too much, the extreme outliers must be removed. Next the photon rate at the output from the beam combiner must be analyzed for the target. If the atmosphere is

unstable, such as there is cloud cover in the middle of the observation, then the photon rate will drop significantly similar to the NAT counts. However for NAT counts, the photons are measured for the input beam whereas the photon rate is measured for the output beam. The interferometer takes measurements on the fringe which are called coherent scans and then takes measurements off the fringe which are called incoherent scans. The raw data is reduced from the bias correction which contains information for the incoherent scans. The bias corrections are done to correct for the offset of the incoherent scans which are supposed to be zero according to equation 3.4 where if the fringe has no contrast $P_{\max} = P_{\min}$ and the visibility must be zero.

3.2.2 Calibration

Before the interferometric observations can be used to extract astrometrically useful information, the raw squared visibilities need to be calibrated with respect to an external calibrator. The calibrator used for δ Sco is ζ Ophiuchi (FK5622). The calibrator is a star that is unresolved by the interferometer and thus should have a $V^2 = 1$. However, this is not true during the reduction process. So the star is calibrated by its offset to a $V^2 = 1$. The target star is calibrated by this offset as well since the calibrated star is typically very close on the sky to the target star and observed nearly at the same time. This is done so the calibrator and target are viewed through nearly the same atmosphere. The star is calibrated in time meaning that each scan is calibrated with respect to the next scan and so

on. To account for atmospheric changes during the night, the calibration process accounts for variations over time in a well specified "window" between 10 and 80 minutes. For the longer time frame, the atmosphere can affect the calibration more, meaning the V^2 is averaged over a longer time frame and that average can have more of an affect from the atmosphere. For this project, a window of 10 minutes was used.

The fringe that is recorded after the beams from different telescopes are combined is dispersed over many spectral channels ranging from channel 1 to channel 16 which correspond to a wavelength range of 850 to 500 nm, respectively. To obtain astrometric measurements from the calibrated scans, channel 10 which contains the Hα emission (at λ = 656 nm) line from the circumstellar region associated with the primary star, was removed. This is because channel 10 contains extra information on the circumstellar disk and can interfere with determining the separation of the binary. Each night was processed through an initial binary fit program to obtain initial guesses of position of the secondary with respect to the primary star. This was found by obtaining the minimum χ^2 in the χ^2 surface defined by different binary separations and orientations. Once the initial guess was obtained from every night, it was again processed through OYSTER to obtain a fit. In this case, a model fit was performed in OYSTER to the scans to determine the best separation parameters (Appendix A).

3.3 Observational Results

3.3.1 Refined Orbit

Observations obtained on 125 separate nights, in 2000 and between 2005-2011, were reduced using the steps outlined in section 3.2. Once every astrometric measurement produced the individual ρ and θ values for each of the 125 nights, it was read into OYSTER (Appendix A). The radial velocities of the primary star were required (Miroshnichenko et al., 2001), as well as the parallax of the system, to determine the primary star's mass. The radial velocities are how the star's Doppler shift is seen due to the rotation about the center of mass. Since the primary star is the more massive and brighter star, this system is a single lined spectroscopic binary system, meaning the radial velocities correspond to the Doppler shift of the primary star. This shift is very apparent when the secondary is very close to the primary during the periastron passage (Figure 3.4). The spectroscopic radial velocities were recorded during the last periastron passage in 2000 by Miroshnichenko et al. (2001) (Appendix B). An offset of -7 m/s was added since that was the best estimate of the systemic velocity (Evans, 1967).

The radial velocities are read into OYSTER along with the parallax. Initial guesses for the seven orbital parameters are also read in (Appendices C.1 and C.2 used for obtaining the best fit). Once the orbital parameters are read in to OYSTER (using double.model from Appendix C.1), the orbital parameters are fit. A best-fit with a reduced χ^2 of 0.686 was

obtained. Table 3.1 contains the best-fit orbital parameters obtained in this study along with previously published orbital parameters as well as newly published work by Meilland et al. (2011) which used the data obtained from this work to fit a binary orbit.

The parameter that was most significantly revised was the period. This particular parameter is the most important to determine the timing of the periastron passage in

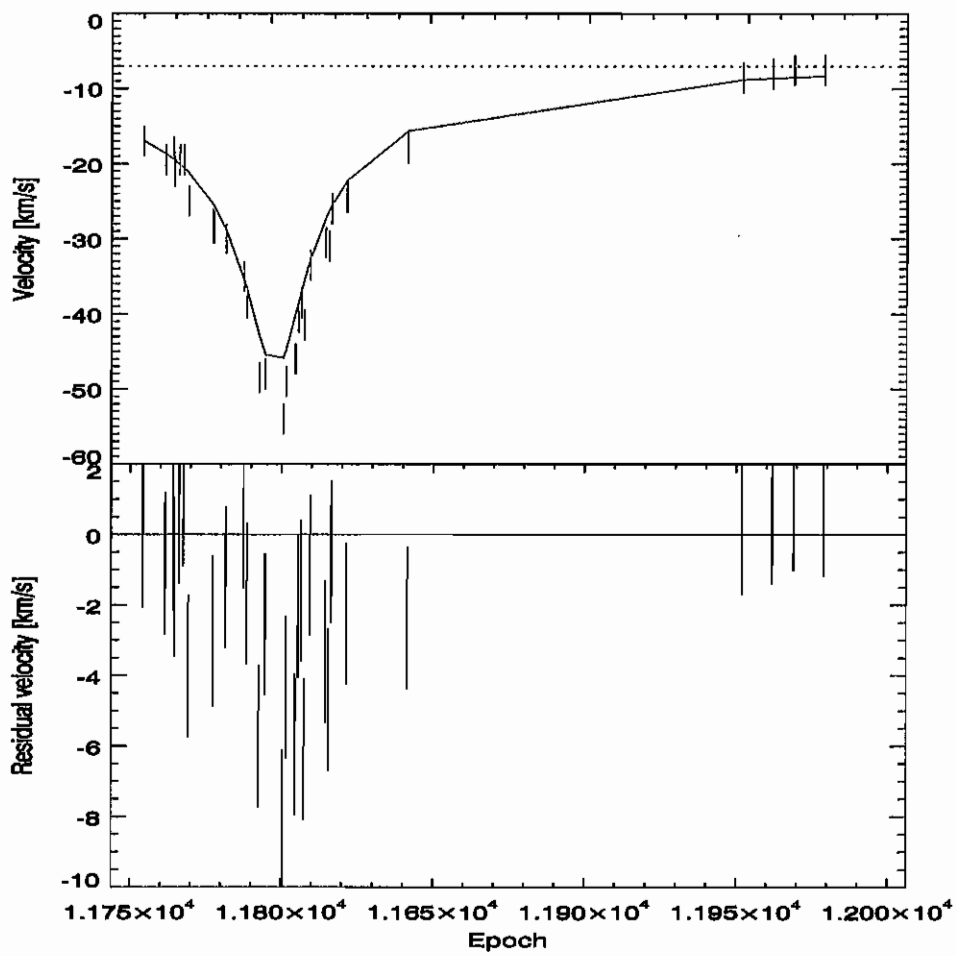

Figure 3.4. Radial velocities of the system, plotted against the epoch, from Miroshnichenko et al. (2001). Included are the residual velocities determining how good a fit the orbital parameters are to the data.

Table 3.1. The orbital elements for δ Sco.

Orbital Parameters	Mason et al. (2009)	Miroshnichenko et al. (2001)	Tango et al. (2009)	This Work	Melland et al. (2011)[c]
P (year)	10.68 ± 0.05	10.58[a]	10.74 ± 0.02	10.809 ± 0.002	10.811 ± 0.01
a (mas)	104 ± 6	107[a]	98.3 ± 1.2	99.0 ± 0.04	98.74 ± 0.07
i (deg)	39 ± 8	38 ± 5	38 ± 6	31.7 ± 0.3	30.2 ± 0.7
Ω (deg)	153 ± 9	175[a]	175.2 ± 0.6	172.8 ± 0.08	174.0 ± 2.5
e	0.94[b]	0.94 ± 0.01	0.9401 ± 0.0002	0.939 ± 0.0007	0.9403 ± 0.0008
ω (deg)	29 ± 12	-1 ± 5	1.9 ± 0.1	2.1 ± 0.07	0.7 ± 2.9
T_0	J2000.693[2]	J2000.693± 0.008	J2000.69389± 0.00007	J2000.6927± 0.005	J2000.6941± 0.003
Periastron Date	2011-05-17 ± 18d	2011-04-10[a]	2011-06-08 ± 7d	2011-07-05 ± 1d	2011-07-05 ± 4d

Notes.
[a]Parameter adopted from Hartkopf et al. (1996) solution.
[b]Parameter adopted from Miroshnichenko et al. (2001) solution.
[c]Data used from this work.

the summer of 2011. A month makes a significant difference where the secondary is located with respect to the primary star. Due to Kepler's second law, the secondary star is moving much more quickly as it approaches the periastron passage (section 2.1), thus if astronomers wish to observe the system, the date of the periastron passage needs to be very precise (Figure 3.5). The reason the periastron date needs to be well known is because most astronomers cannot get extended periods of time, such as a month or two, on a telescope. Typically, the time allocated on a telescope is on the order of a week or two. So since the binary is moving so quickly near the periastron, a date needs to be determined within a week of when it occurs so the possible interaction between the primary, secondary, and circumstellar disk can be observed.

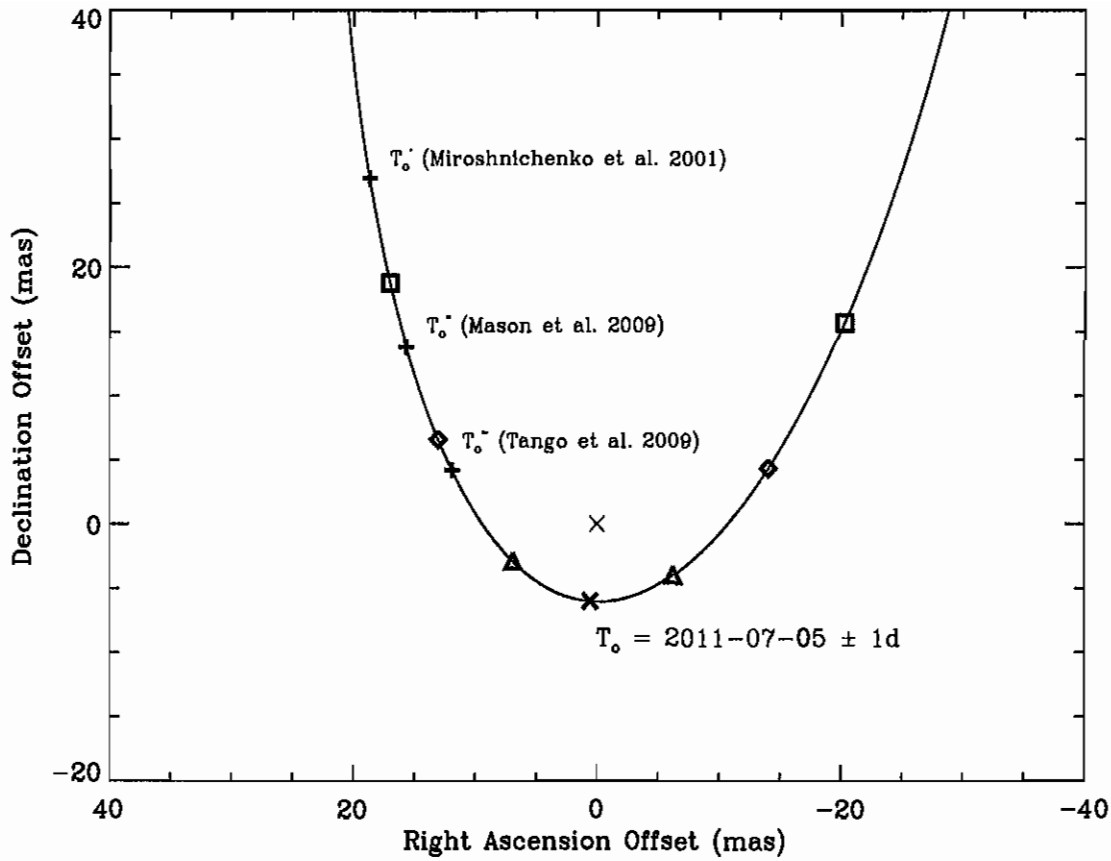

Figure 3.5. The periastron passage marked with an X. The predicted positions of the secondary are plotted on the orbit 10 days (triangle), 30 days (diamond), and 60 days (box), before and after the periastron passage. Locations of the secondary along the newly revised orbit from previous periastron results are shown (pluses).

For this particular system, the orbital parameters were in need of a revision since NPOI data compared to previous results did not agree with the previously determined orbits (Figure 3.6 for a comparison of the orbits found by Miroshnichenko et al. (2001), Mason et al. (2009), Tango et al. (2009), and and this work). The revised date for the periastron passage was calculated to be U.T. 2011-07-05 ± 1 day.

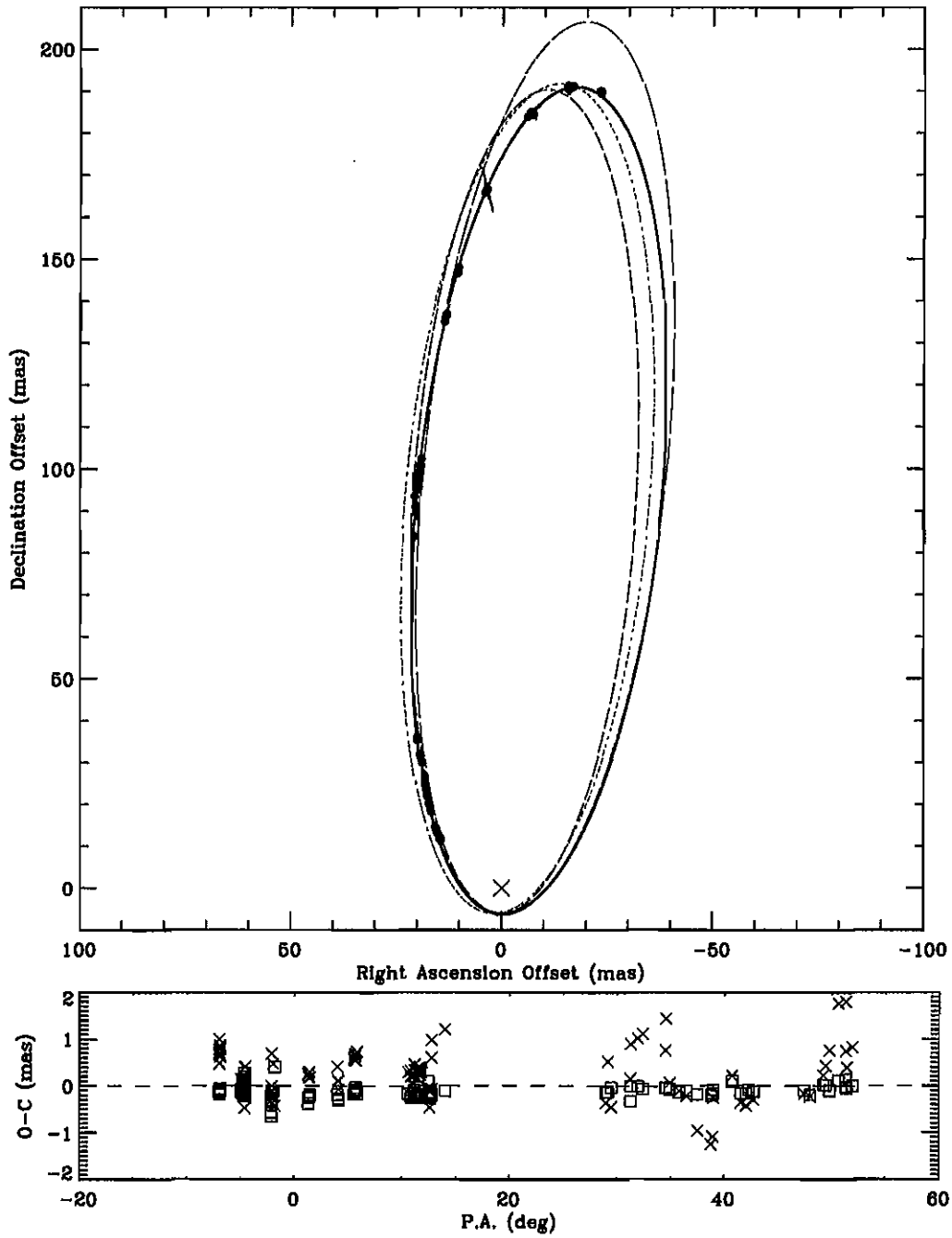

Figure 3.6. Top: binary orbits based on orbital parameters obtained from this paper (solid, blue), Tango et al. (2009) (orange, dashed), Mason et al. (2009) (light blue), and Miroshnichenko et al. (2001) (green). The filled, black circles are the astrometric results. The error ellipses are plotted over the data points (red). The locations of the primary is marked with an X. Bottom panel: The east-west (squares) and north-south (crosses) represent the O-C vectors as a function of P.A. of the secondary.

3.3.2 Errors on ρ_{min}

Another important parameter that was needed was the minimum separation between the primary and secondary during the periastron passage in 2011. This was especially important to find so it could be determined whether the secondary would come close enough to the primary star to cause a possible collision between the circumstellar disk and the secondary. This is all dependent on the minimum separation and size of the disk (the next chapter for disk size). The errors for the ρ_{min} were obtained using a Monte-Carlo algorithm. Each orbital parameter that determines the apparent orbit (Ω, ω, i, e, and a) had 300,000 numbers randomly generated with the mean value centered around the best-fit value and the width corresponding to the errors on each parameter. Each parameter was run through another program called orbits.pro to create an individual orbit based on the parameters (Appendix D.2). Once each orbit was created, the minimum ρ was found in the apparent orbit. Since astronomers want to view the interaction between the primary and secondary, in the apparent orbit, it is customary to report on the ρ_{min} values. In the case of δ Sco, ω is very close to zero and this implies that ρ_{min} in the true orbit is the same as ρ_{min} in the apparent orbit. Once each ρ_{min} was determined, it stored and plotted the synthetic data points in a histogram and a Gaussian was fit to the distribution. From the Gaussian, a mean value and standard deviation was determined, thus an error on the separation was determined. This error was calculated using all the errors found from the binary parameters

(Table 3.1) which assigns an uncertainty to ρ_{min} (Figure 3.7 for the Gaussian distribution).

The closest approach for the periastron passage is $\rho_{min} = 6.04 \pm 0.07$ mas.

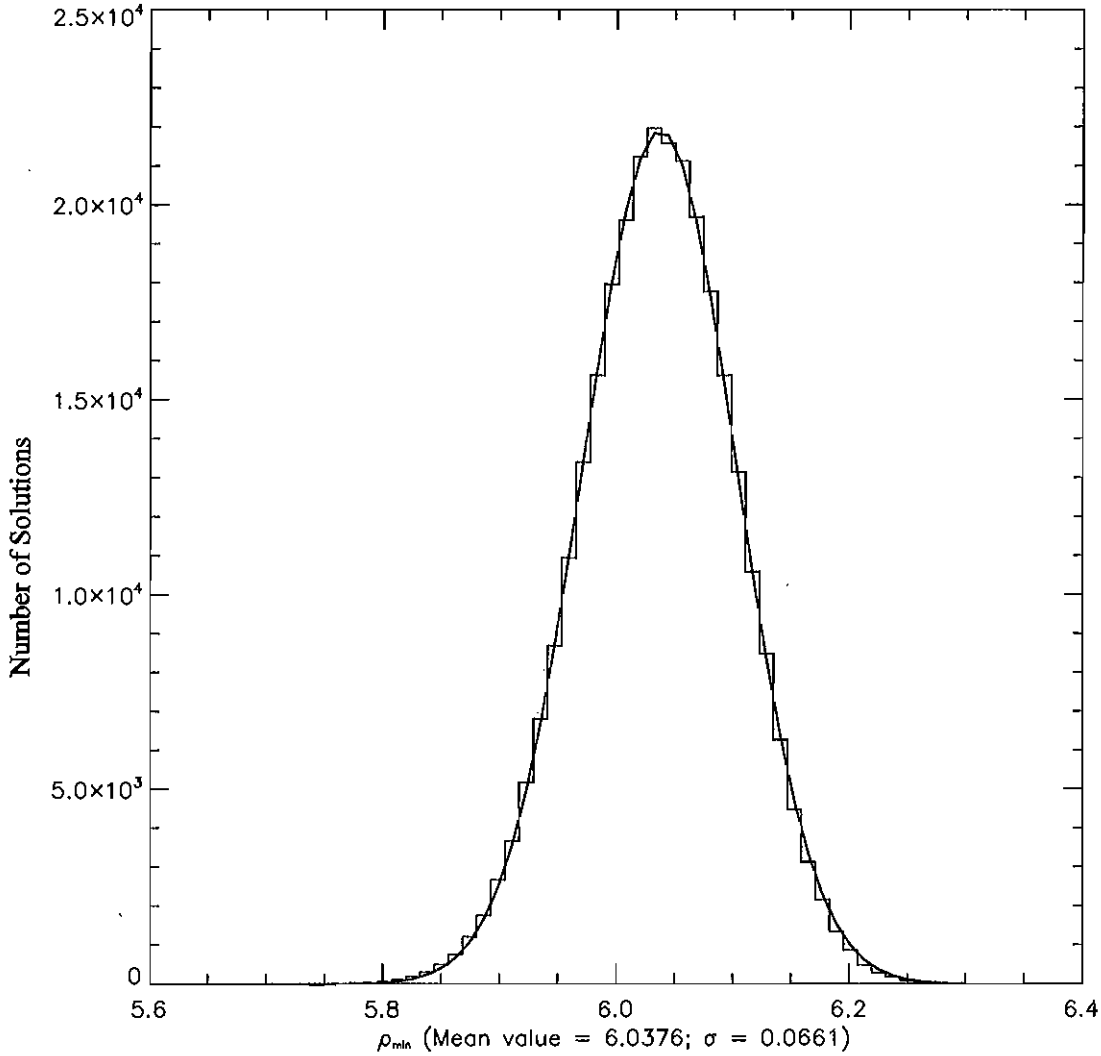

Figure 3.7. Histogram of solutions obtained for the apparent separation of the secondary and primary star during the periastron passage, based on 300,000 synthetic data sets.

CHAPTER IV

CIRCUMSTELLAR DISKS

4.1 Background

Collins (1987) gave the definition of a Be star as "a non-supergiant B-type star whose spectrum has or had at some time, one or more Balmer lines in emission." Be stars typically rotate close to their critical limit where the centrifugal force produced by the spin balances the gravity of the star. Studies have shown that the distribution of known Be stars peak at values of 70-80% of the critical rotational velocity (Porter, 1996). It is widely accepted that the contribution from rotational velocity close to the critical limit does have an effect on the development of the circumstellar (CS) disk. However, whether this is the only mechanism in the creation of a disk, or if there are other processes involved, is still not fully understood. A general consensus is that Be stars are rapidly rotating B-type stars that produce a disk in their equatorial plane. CS disks are *not* related to the natal disk the star had during it's accretion phase (Porter & Rivinius, 2003).

To measure the rotational rates of Be stars, the line-width velocity is measured. The rotational rate of the star is given by v, known as the equatorial velocity, however, the measured quantity is $v\sin i$ due to the the inclination angle which causes the rotational velocities to be projected onto the line of sight. Stars with rotational velocities above the 80% critical value are likely to produce underestimates of the true rotational speed of the

star (Collins & Truax, 1995). Since the Be type star rotates so close to the critical limit, the rotation is an important contribution of the formation of a CS disk.

The most common emission lines in a Be star are those of HI, HeI, FeII, and sometimes SiII and MgII (Porter & Rivinius, 2003). A well-known issue is that the stars are highly variable and can lose their disk completely and thus their emission lines. They can maintain emission lines on long (months to years) to short (days or less) time-scales, where the Be characteristic disappears completely only to return years later (Cote & van Kerkwijk, 1993). Spectroscopic observations determine whether the emission line profiles are either single or double-peaked. Most common are the double-peaked profiles and typically they are symmetric across the line center and usually of equal height (Hanuschik et al., 1996). Depending on the amount of CS material, the disk becomes dominated by free-free and free-bound emission in the near- to mid-infrared regions (Doazan et al., 1991).

Cote & van Kerkwijk (1993) divide Be stars are into different classifications. The stars of groups I-IV are stable, meaning over a period of 20 years, emission lines were always present during observation of the spectrum. Group I stars have very strong Balmer lines and FeII emission lines. Group II-IV have much weaker Balmer emission lines. Group V stars lost their emission features at least once during the 20 year period, changing from B to Be or vice versa.

Optical interferometry has started to play a big role in resolving many Be stars and determining their disk structures. Thanks to long-baseline interferometry it has been shown that CS emission originates in a disk-like structure around the star (Tycner et al., 2005).

Numerical models fitted to observations have determined that the density of the disk falls off as a $\rho = r^n$, where r is the radial distance from the axis of rotation (Waters, 1986). Typically these models are fit to the IR continuum and results suggest the index, n is between 2 and 4 (Waters, 1986; Carciofi et al., 2006). Models were created to describe how the gas, in a viscous disk, is transferred to the outer part of the disk. The viscosity of the disk plays a role in transferring momentum from the inner parts of the disk to the outer regions, otherwise the gas would orbit the star forever (Carciofi et al., 2006).

Some Be stars are thought to form in binary systems where mass transfer was influenced at one time by the secondary companion. The mass transfer, in turn, is responsible for spinning up the primary star (Gies, 2000). However, the binary system has to be a close system, i.e. the secondary has to pass close enough to the primary Be star, such that the mass transfer can actually occur. Since not all Be stars are known binaries, it is unlikely that the binary mass transfer mechanism is responsible for Be phenomenon in all stars.

4.1.1 The Circumstellar Disk of δ Sco

The δ Sco system has been of great interest to the astronomical community. It was first discovered by Innes (1901). Cote & van Kerkwijk (1993) rediscovered the system and found a faint Hα emission from the primary. Porter & Rivinius (2003) remark that a system such as δ Sco maybe classified as a "close system" due to the high eccentricity of the system which leads to a non-negligible tidal interaction during the periastron passage. However, Miroshnichenko et al. (2001) determined that the primary is unlikely to fill the Roche lobe during a periastron passage due to the distance between the two stars being too great even at the closest approach, but did agree that the tidal interactions due to close proximity might cause mass loss of the primary star.

In June of 2000, Otero et al. (2001) observed that the Hα emission was fully developed before the system began brightening. The disk formed or grew before the periastron passage and kept growing. The corresponding Hα intensity increase during the two months before the periastron passage suggests that the optical depth of the disk was increasing and contributed to the system's overall intensity. As the secondary moved closer to the primary during the last periastron passage in 2000, the disk stopped growing in size and due to the large optical depth of the disk, it caused an overall fading of the system (Miroshnichenko et al., 2001). Miroshnichenko et al. (2001) suggested that as the secondary moved away, the disk was allowed to grow again, which implies that the periastron plays an important

role in the disk growth and mass loss of the primary. Since the separation at the closest approach is still too great between the primary and secondary, there is no mass transfer to the secondary via the Roche lobe. This is due to the fact that the secondary moves too quickly around the periastron and does not give the primary enough time to fill its Roche lobe, thus not allowing a mass transfer to occur between the primary and secondary (Miroshnichenko et al., 2001).

The Hα emission is the strongest emission line, and therefore gives the most reliable radial velocities (RV). Since the disk is formed around the primary star, it moves with the primary star and should reflect the star's motion (Miroshnichenko et al., 2001). The primary star's systemic velocity is highly affected by the periastron passage, due to the components' acceleration, the most accurate measurement of the systemic velocity was obtained when the components had large separation and has a value of -7 km s^{-1} (Evans, 1967). The Hα minimum took place between 2000 September 7 and 12. Miroshnichenko et al. (2001) observed that the emission line spectrum was strong in 2000, implying that the disk grows with time.

Miroshnichenko et al. (2003) observed the system after the last periastron passage and found that emission lines of HI of Balmer (Hα-Hδ) and Paschen (P13-P16), HeI, FeII, and SiII were present during all observations. They also observed that the disk emission

was double-peaked, suggesting that the CS matter has a disk-like distribution. Miroshnichenko et al. (2003) estimates that the disk is probably Keplerian with an outer radius of $\sim 10\ R_*$ where $R_* = 7.0 R_\odot$ with a $v\sin i$ = 148 km s^{-1} and a $v_{\rm rot} = 240$ km s^{-1} which is $\sim 40\%$ of the critical rotation speed ($v_{\rm crit} = 620$ km s^{-1} for a primary whose mass is $15 M_\odot$ and radius $7 R_\odot$).

Other studies were done in the IR continuum. Banerjee et al. (2001) observed the system in the near-infrared and determined that the star showed an excess of IR radiation which is produced from free-free and free-bound emission in the CS disk. The contribution to the star from the disk depends on the density, temperature, and ionization degree throughout the disk. If the Hα line has a strong emission, this usually correlates with strong IR emission as well. Carciofi et al. (2006) analyzed photometric observations in the mid-infrared (10 μm and 18 μm) from 2000-2005 as well as optical spectropolarimetry (blue: 3190-6050 Å and red: 5960-10410 Å). They determined the disk characteristics with a density of $\rho_o = 4.5\text{x}10^{-10}$g cm^{-3} and size of $R_{\rm disk} = 7 R_*$ which implied a very small but dense disk. Carciofi et al. (2006) determined that along the mid-plane, the temperature is at a minimum of 7,000K ($\sim 4 R_*$) to a maximum of $\sim 30,000$K near the base of the disk at the surface of the star. Halonen et al. (2008) solutions agree with the results of Carciofi et al. (2006) within errors, however, they could not find a good model-fit for the orientation and structure of the disk. The most recent observations of the disk in the IR continuum were

obtained by Millan-Gabet et al. (2010) with a size of 2.2 ± 0.4 mas in HeI and 1.9 ± 0.3 mas in Brγ which are 2.0583 μm and 2.1657 μm wavelengths respectively. However, they state that the optical depth in Hα is likely to be much larger than in either HeI or Brγ, and therefore the disk will look much larger in Hα.

Meilland et al. (2011) has recently studied the system from 2007-2011, obtaining observations in the visible and infrared regions. They specifically observed the Hα, HeI (2.06 μm) and Brγ. As these lines are formed at different distances from the star, they will report different sizes for the disk. The sizes that were obtained from the data include Hα: 4.8 ± 1.5 mas, Brγ: 2.9 ± 0.5 mas, and HeI: 2.4 ± 0.3 mas. Meilland et al. (2011) also did observe that the disk is rotating with a brighter emitting region in the blue part of the line (i.e., the part moving towards the observer) and a fainter region in the red part (i.e. moving away from the observer). However, the emitting regions are symmetric with respect to the central star. They concluded that the binarity of the system will play an important role in the shaping of the disk.

4.2 Determining Disk Characteristics

A binary signature can be represented by a cosine function (eq. 3.14 and Figure 3.1). The interferometric data obtained from NPOI are acquired over many spectral channels which correspond to different wavelengths. Each channel that is used is averaged over the $\Delta\lambda$ band-pass. Channel 10 contains the Hα emission line and therefore will contain

(in addition to the binary signature) the signature due to the circumstellar disk. Therefore, compared to the other 15 channels, the squared visibility in channel 10 is expected to be lower due to the contribution from the disk. In this case, the only information that is needed to be extracted is the Hα signature from the disk contained in channel 10. However, the squared visibility signature contains signatures from the primary star, secondary star (the binary signature), as well as the disk structure. To get only disk parameters, the cosine signature needs to be properly removed from each scan (Figure 3.1).

The problem that arises is that $\tilde{V}_{\text{binary}}$ and $\tilde{V}_{\text{disk}}$, the visibility of the binary signature and the disk, respectively, might be complex quantities. The data is in V^2 format only and therefore the complex quantities, $\tilde{V}$, cannot be extracted directly from V^2. However, a number of approximations can be made such that both of these quantities can be represented by real numbers. For example, by assuming that the disk structure can be represented by a point-symmetric flux distribution, the quantity $\tilde{V}^2_{\text{disk}}$ becomes real ($\tilde{V}^2_{\text{disk}} = V^2_{\text{disk}}$). Another approximation that can be made is that $\tilde{V}^2_{\text{binary}}$ is a real quantity as well. The reason that $\tilde{V}^2_{\text{binary}}$ can be imaginary is due to the phase factor that occurs from the phase associated with the binary system. This phase, $\Phi(\Delta m, \Delta x, \Delta y, ...)$ is a function of Δm which is the magnitude difference between the two components as well as the projected separation and spatial frequency. The most simple approximation is when the primary and secondary are along the same line, in this case, along what we denote the north axis (Figure 4.1). Since

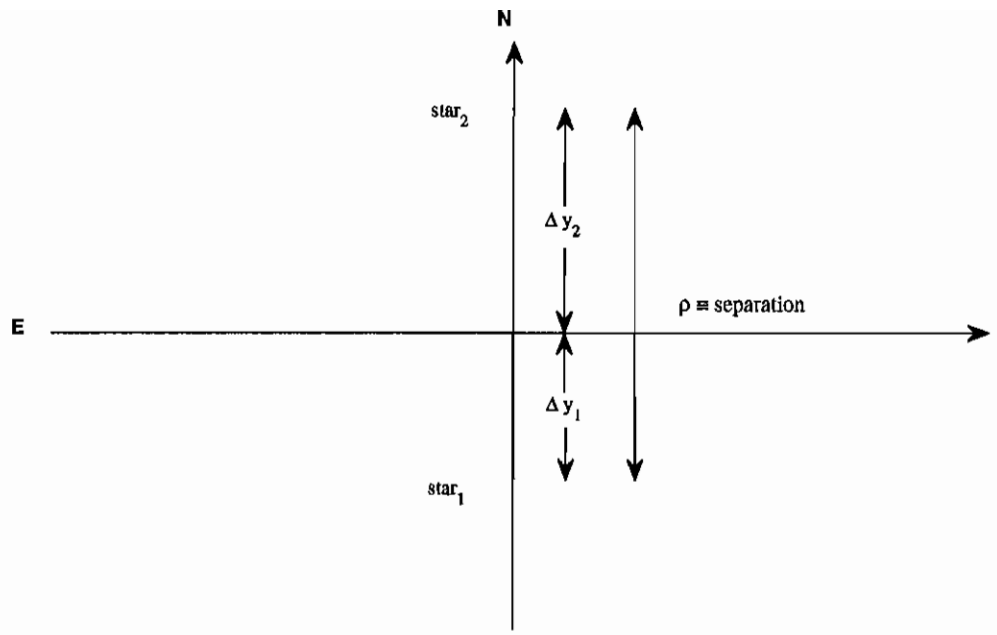

Figure 4.1. A schematic representation of the binary system along the North axis.

stars can be represented by delta functions, the Fourier Transform to the spatial frequency space of two delta functions at Δy_1 and Δy_2 is

$$F_{\text{star1}}[\delta(y-\Delta y_1)] = \int_{-\infty}^{+\infty} V_1 e^{-2\pi i s y}\delta(y-\Delta y_1)\,dy = V_1 e^{-2\pi i s \Delta y_1}, \tag{4.1}$$

and

$$F_{\text{star2}}[\delta(y-\Delta y_2)] = \int_{-\infty}^{+\infty} V_2 e^{-2\pi i s y}\delta(y-\Delta y_2)\,dy. = V_2 e^{-2\pi i s \Delta y_2}. \tag{4.2}$$

The phase components in the spatial frequency spaces can be represented by

$$\phi_1 = 2\pi\,\Delta y_1 s, \tag{4.3}$$

$$\phi_2 = 2\pi\, \Delta y_2 s, \tag{4.4}$$

where $s = B/\lambda$, is the spatial frequency, B is the baseline length, and λ is the wavelength. The complex visibilities associated with the two stars then become

$$\tilde{V}_{\text{star1}} = V_1\, e^{-i\phi_1}, \tag{4.5}$$

$$\tilde{V}_{\text{star2}} = V_2\, e^{-i\phi_2}. \tag{4.6}$$

The origin in Figure 4.1 is at the flux weighted center, which requires that

$$y_c = \frac{F_1\, \Delta y_1 + F_2\, \Delta y_2}{F_1 + F_2} = 0. \tag{4.7}$$

The separation between the two stars is given by

$$\rho = \Delta y_2 - \Delta y_1. \tag{4.8}$$

Taking equation 4.7 and solving for Δy_1 and replacing it in equation 4.8, an expression for Δy_2 is obtained

$$\Delta y_2 = \frac{\rho}{1+K}, \tag{4.9}$$

and similarly solving for Δy_1 gives

$$\Delta y_1 = \frac{-K\rho}{1+K}. \tag{4.10}$$

Using equations 4.9 and 4.10 and inserting them into equations 4.3 and 4.4 allows the complex phases to be rewritten as

$$\phi_1 = \frac{-K\Psi}{1+K}, \tag{4.11}$$

and

$$\phi_2 = \frac{\Psi}{1+K}, \tag{4.12}$$

where $\Psi = 2\pi\rho s$, which is the phase of the projected separation onto the spatial frequency plane. The visibility of the binary system in the complex plane is illustrated schematically by Figure 4.2, where the normalized (to unity) complex visibility can be written as

$$\tilde{V}_{\text{binary}} = \frac{F_1\tilde{V}_{\text{star1}} + F_2\tilde{V}_{\text{star2}}}{F_1 + F_2}, \tag{4.13}$$

which can be reduced to

$$\tilde{V}_{\text{binary}} = \left(\frac{1}{1+K}\right)\left[\tilde{V}_{\text{star1}} + K\tilde{V}_{\text{star2}}\right], \tag{4.14}$$

where $K = F_2/F_1$ is the flux ratio of the components. Using equations 4.5 and 4.6, the total normalized visibility becomes

$$\tilde{V}_{\text{binary}} = \frac{V_1\, e^{-i\phi_1} + KV_2\, e^{-i\phi_2}}{1+K}. \tag{4.15}$$

Equation 4.15 can also be written as

$$\tilde{V}_{\text{binary}} = \left(\frac{1}{1+K}\right) V_1(\cos\phi_1 - i\sin\phi_1) + KV_2(\cos\phi_2 - i\sin\phi_2). \tag{4.16}$$

Using equations 4.11 and 4.12 to replace the phases ϕ_1 and ϕ_2 results in

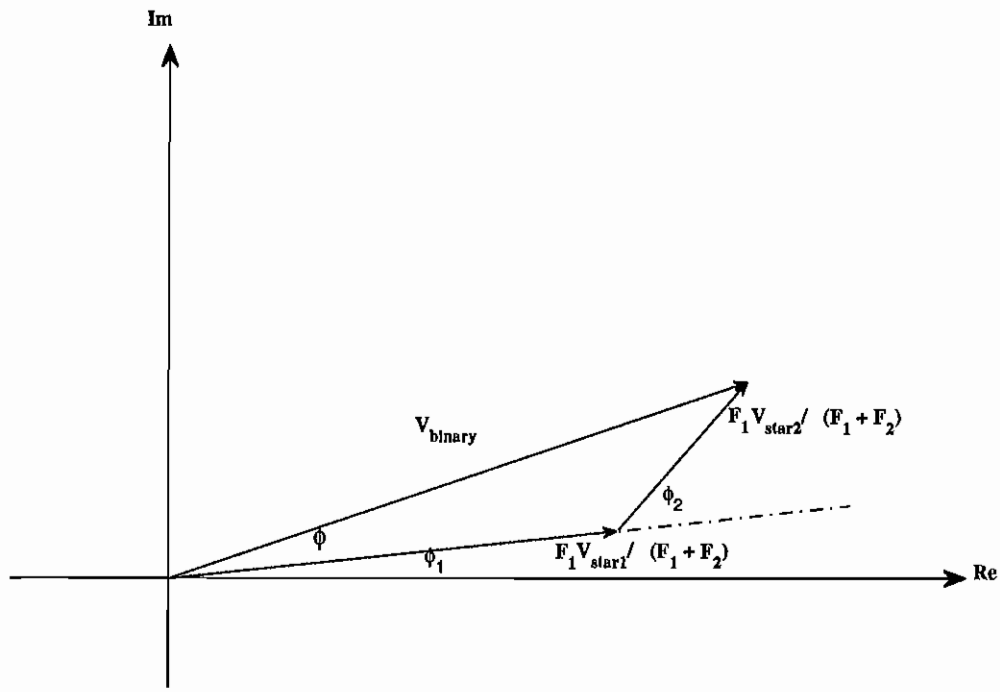

Figure 4.2. A schematic representation of the visibilities of the binary system in the complex plane.

$$\tilde{V}_{\text{binary}} = \left(\frac{1}{1+K}\right)\left[V_1\cos\left(\frac{K\Psi}{1+K}\right) + KV_2\cos\left(\frac{\Psi}{1+K}\right) + i\left(V_1\sin\left(\frac{K\Psi}{1+K}\right) - KV_2\sin\left(\frac{\Psi}{1+K}\right)\right)\right]. \tag{4.17}$$

Because the complex phase of $\tilde{V}_{\text{binary}}$ can be simply obtained from the tangent of the imaginary over the real component $\left(\tan\phi = \text{Im}/\text{Re}\right)$ then

$$\tan\phi = \frac{V_1\sin\left(\frac{K\Psi}{1+K}\right) - KV_2\sin\left(\frac{\Psi}{1+K}\right)}{V_1\cos\left(\frac{K\Psi}{1+K}\right) + KV_2\cos\left(\frac{\Psi}{1+K}\right)}. \tag{4.18}$$

The squared visibility (i.e., the interferometric observable) of the system is found by taking equation 4.15 and multiplying it by its complex conjugate, which yields

$$|V_{\text{binary}}|^2 = \left(\frac{1}{1+K}\right)^2\left[V_1^2 + \left(KV_2\right) + KV_1V_2\left(e^{i(\phi_2-\phi_1)} + e^{-i(\phi_2-\phi_1)}\right)\right]. \tag{4.19}$$

Representing the phase difference $(\phi_2 - \phi_1)$ with Ψ produces a simple expression for the modulus of V_{binary}

$$V_{\text{binary}} = \sqrt{\frac{V_1^2 + (KV_2)^2 + 2KV_1V_2\cos\Psi}{(1+K)^2}}. \tag{4.20}$$

We note that equation 4.18, representing the phase, is in agreement with Mourard et al. (1992), but equation 4.20, for the visibility modulus, is slightly different which we attribute to typographical errors in their paper.

We can model the interferometric signature in the Hα channel as

$$V_{\mathrm{H}\alpha}^2 = (c_{\mathrm{p}} V_{\mathrm{binary}} + (1 - c_{\mathrm{p}}) V_{\mathrm{disk}})^2, \tag{4.21}$$

or

$$V_{\mathrm{H}\alpha}^2 = c_{\mathrm{p}}^2 \mathrm{V}_{\mathrm{binary}}^2 + (1 - c_{\mathrm{p}})^2 \mathrm{V}_{\mathrm{disk}}^2 + 2c_{\mathrm{p}}(1 - c_{\mathrm{p}}) \mathrm{V}_{\mathrm{disk}} \mathrm{V}_{\mathrm{binary}}, \tag{4.22}$$

where c_{p} is the fractional photospheric contribution from the stars and is between [0,1] and $1 - c_{\mathrm{p}}$ is the contribution only from the disk. The values for c_{p} can be obtained from

$$c_{\mathrm{p}} = \frac{F_{\mathrm{stars}}}{F_{\mathrm{stars}} + F_{\mathrm{H}\alpha}} \leq 1, \tag{4.23}$$

where F_{stars} and $F_{\mathrm{H}\alpha}$ are the total flux from the two stars and from the disk, respectively. F_{stars} can be approximated by the width of channel 10 (W_{10}), corrected for the absorption component from the stars (W_{abs}) and $F_{\mathrm{H}\alpha}$ can be described by the equivalent width of the Hα emission line ($E_{\mathrm{H}\alpha}$), in which case

$$c_{\mathrm{p}} \approx \frac{W_{10} - \mathrm{W}_{\mathrm{abs}}}{W_{10} + E_{\mathrm{H}\alpha}}, \tag{4.24}$$

where W_{10} is 15 nm $\pm$ 1 nm and the equivalent width of the Hα emission from the disk are listed in Table 4.1 for different observational epochs. The absorption component, W_{abs},

was calculated to be 0.283 ± 0.01287 nm using the formula

$$W_{\rm abs} = (18.02 \pm 1.03)(B-V)_0 + (8.06 \pm 0.17) \tag{4.25}$$

obtained from Cote & Waters (1987). A $(B-V)_0$ of -0.29 was used from Tango et al. (2009). Each $c_{\rm p}$ calculated was obtained from average equivalent width values taken from spectroscopic observations obtained as part of the study presented by Jones et al. (2011) and Meilland et al. (2011) (Table 4.1). In previous models, there was an attempt to try

Table 4.1. The Hα equivalent widths and the corresponding $c_{\rm p}$ values

Year	**Hα EW (nm)**	$c_{\rm p}$
2005	-2.798 ± 0.0838^a	0.8269 ± 0.0103
2006	-1.567 ± 0.0421^a	0.8883 ± 0.0071
2007	-1.430 ± 0.0430^a	0.8957 ± 0.006
2008	-1.430 ± 0.0430^a	0.8957 ± 0.006
2009	-1.430 ± 0.0430^a	0.8957 ± 0.006
2010	-0.7 ± 0.1^b	0.9374 ± 0.0037
2011	-0.7 ± 0.1^b	0.9374 ± 0.0037

Notes.
[a]Equivalent width adapted from Jones et al. (2011).
[b]Equivalent width adapted from Meilland et al. (2011).

to divide out the binary contribution from the Hα channel, however, since there are cross terms in the equation 4.22, $V^2_{\rm binary}$ cannot simply be divided out of the equation. Due to the cross-term problem, it was necessary to develop another method to better extract disk properties. Instead of dealing with squared visibilities throughout the entire calculation, we would instead take the square-root of the squared visibilities initially and deal only with

the visibilities. Strictly speaking, this is valid if the two components, V_1 and $V_{H\alpha}$, have the same complex phase.

In the Hα channel (channel 10) the visibilities have an additional contribution from the disk, $V_{H\alpha}$ which is added onto and along the V_1 vector because the disk contributes to the primary star (Figure 4.3). The figure shows that since $V_{H\alpha}$ is parallel to V_1 (i.e., the

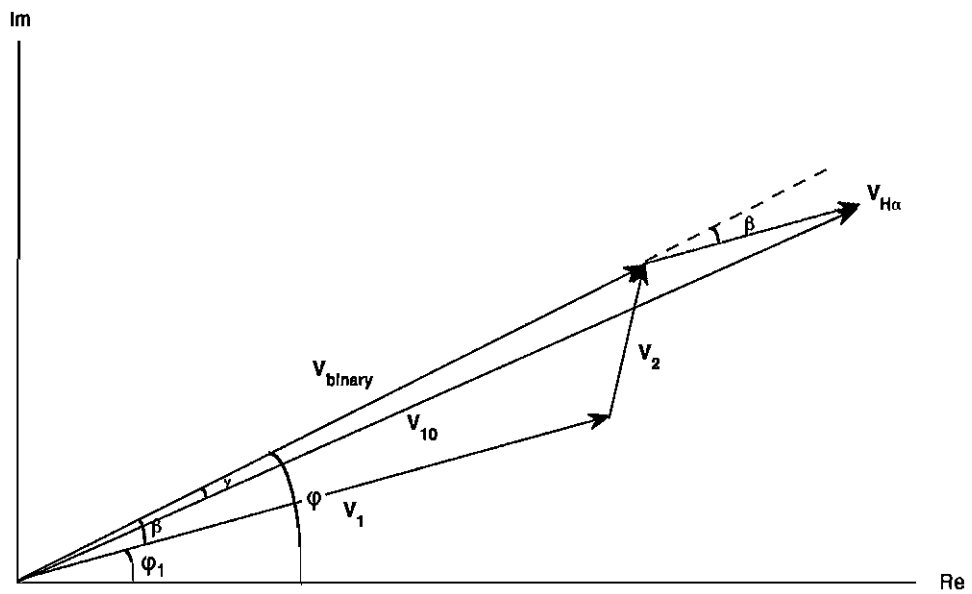

Figure 4.3. A schematic representation of the binary system where $V_{H\alpha}$ is parallel to V_1.

circumstellar disk is concentric with the primary star), it will deviate from V_{binary} by angle β, which is the angle between V_{binary} and V_1. The total visibility component measured is V_{10} that is the sum of all three components (two stars and the disk). δ Sco has a $\Delta m \approx 2.2$ (Tango et al., 2009), which implies that the secondary is approximately 10% as bright as the primary and if both stars are spatially resolved at a similar level, then $V_2 \approx 0.1V_1$. More specifically, the visibilities associated with the individual stars can be well described by a

Fourier Transform of a Uniform disk (UD) model

$$V_{\mathrm{UD}} = \frac{2J_1(\pi\,\theta_{\mathrm{UD}}\,s)}{\pi\,\theta_{\mathrm{UD}}\,s}, \tag{4.26}$$

where the uniform disk diameter, θ_{UD}, is 0.45 ± 0.04 mas and 0.2 mas (nearly unresolved) for the primary and secondary respectively (Tycner et al., 2011). The angle between V_{binary} and V_{10} is γ which is less than β. To determine the biggest deviation β is from V_1, we took the total phase of the system, which is the complex angle associated with V_{binary} (ϕ) and subtracted the phase of V_1 (ϕ_1) (Figure 4.4). To calculate the phase of V_1 we set $V_2 = 0$ in equation 4.18, which represents a completely resolved star and we obtain

$$\tan\phi_1 = \frac{\sin\left(\frac{K\Psi}{1+K}\right)}{\cos\left(\frac{K\Psi}{1+K}\right)}. \tag{4.27}$$

This allows for the flux weighted center to remain at the same location between the two stars, but for the secondary star to not contribute to the overall phase. The total phase was subtracted from the V_1 phase and the resultant angle was β (Figure 4.4). Figure 4.5a shows that β scales as Δm gets smaller which is due to the visibility vector of the secondary becoming comparable to the visibility vector of the primary star. As seen in Figure 4.5b, the maximum value for over several projected separations, 192.92 mas being the largest

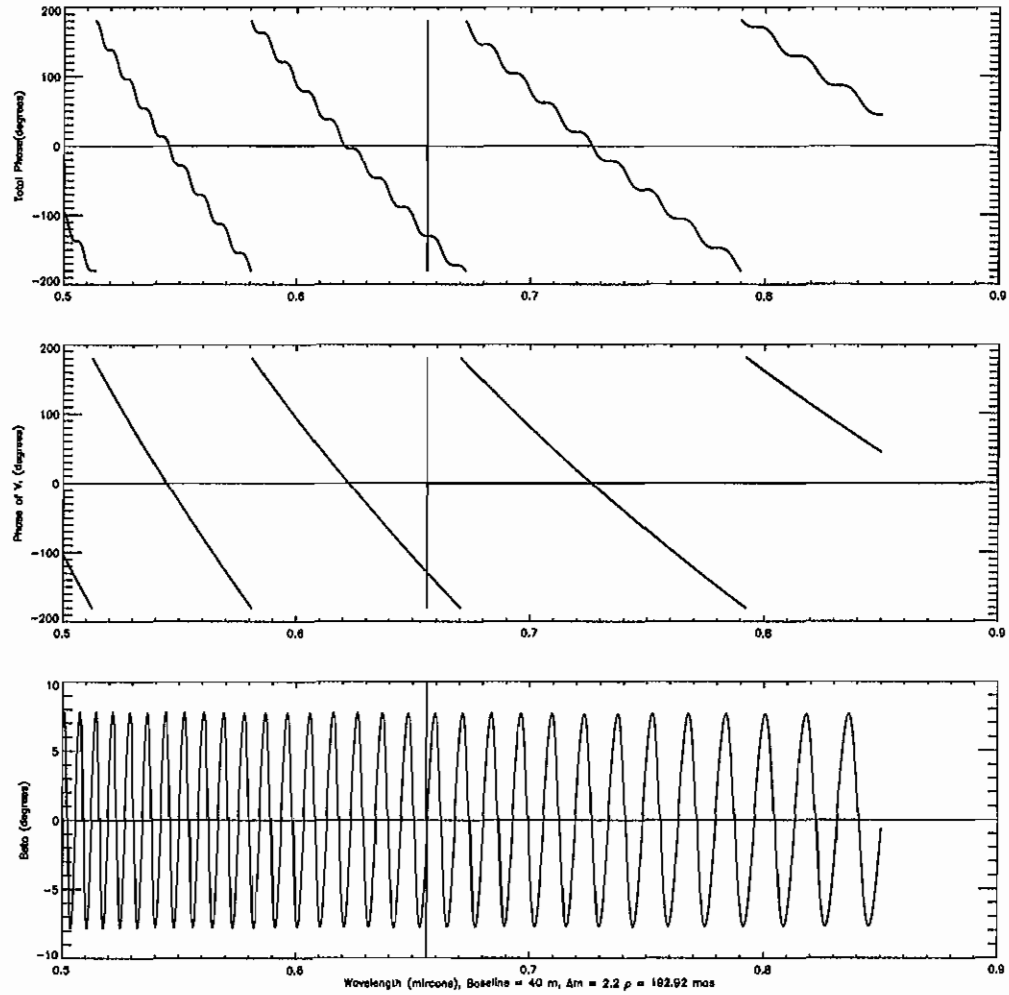

Figure 4.4. The total phase, ϕ, is plotted in frame 1. The phase contribution from V_1 is plotted in frame 2. Frame 3 contains the resulting phase subtraction β. The phase is plotted as a function of wavelength, with a baseline length of 40 m, an apparent separation of 192.92 mas and a Δm of 2.2 (Tango et al., 2009).

separation of the binary system (Figure 3.6), was 8° (Figure 4.4). As can be seen in Figure 4.5b, the frequency of β increases with projected separation, but the maximum angle remains the same for different separations.

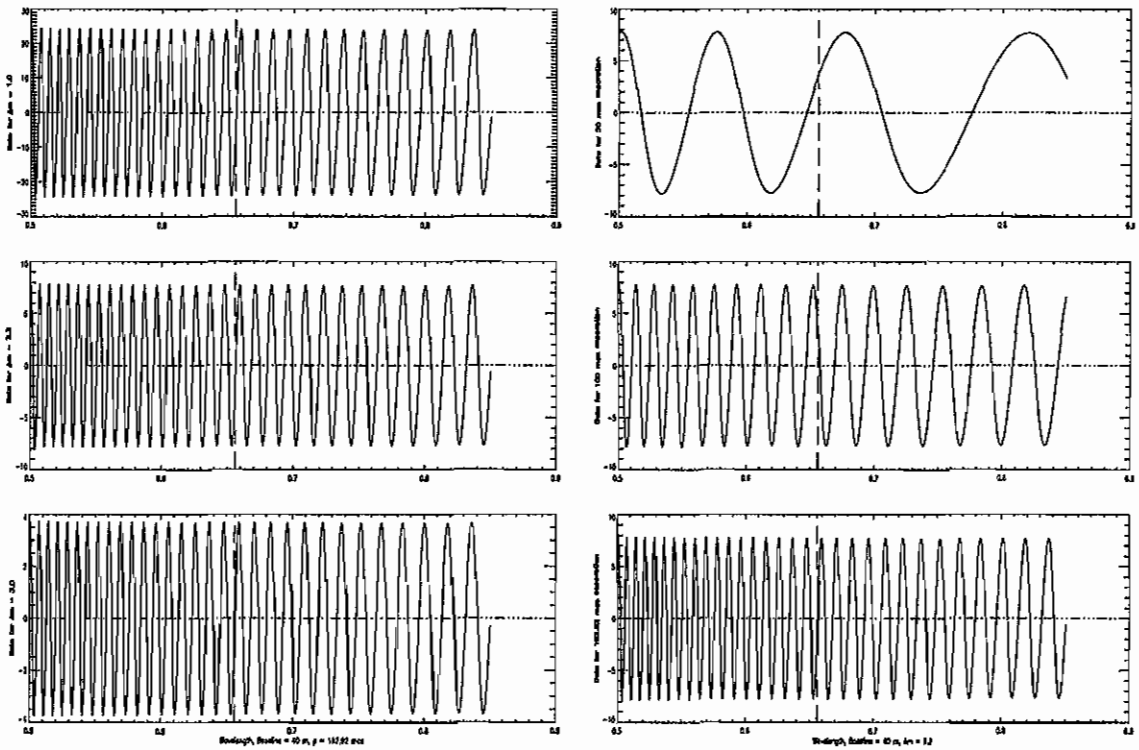

(a) Δm = 1.0, 2.2, 3.0 (b) ρ = 20, 100, 192.92 mas

Figure 4.5. Panel (a): A comparison of how the Δm affects the β angle. Δm includes 1.0, 2.2, and 3.0 respectively, with a baseline of 40 m and apparent separation of 192.92 mas. Panel (b): A comparison of how the projected separation affects the frequency of the β angle. The separation includes 20, 100, and 192.92 mas respectively with a baseline of 40 m and Δm of 2.2 (Tango et al., 2009).

As long as β is small, we can neglect the fact the V_{binary}, $V_{\text{H}\alpha}$, and V_{10} are not all along the same line in Figure 4.3 and approximate the results by assuming that $\beta = 0$. By making this approximation, equation 4.21 becomes

$$\mathrm{V}_{10} = \sqrt{(c_{\mathrm{p}}\mathrm{V}_{\text{binary}} + (1-c_{\mathrm{p}})\mathrm{V}_{\text{H}\alpha-\text{approx}})^2}, \tag{4.28}$$

$$= c_{\mathrm{p}}\mathrm{V}_{\text{binary}} + (1-c_{\mathrm{p}})\mathrm{V}_{\text{H}\alpha-\text{approx}}, \tag{4.29}$$

where we can solve for $V_{H\alpha-approx}$, which becomes

$$V_{H\alpha-approx} = \frac{V_{10} - c_p V_{binary}}{(1 - c_p)} \tag{4.30}$$

To determine how much β affects the results, the error must be calculated. If the angles are taken into account the expression for visibility amplitude in channel 10 would be

$$V_{10} = c_p V_{binary} \cos\gamma + (1 - c_p) V_{H\alpha} \cos\beta, \tag{4.31}$$

and solving for $V_{H\alpha}$ gives

$$V_{H\alpha} = \frac{V_{10} - c_p V_{binary} \cos\gamma}{(1 - c_p)\cos\beta}. \tag{4.32}$$

The difference between equations 4.30 and 4.32 is

$$V_{H\alpha} - V_{H\alpha-approx} = \frac{V_{10}}{(1 - c_p)}\left[\frac{1}{\cos\beta} - 1\right] - \left[\frac{c_p}{(1 - c_p)}\right] V_{binary}\left[\frac{\cos\gamma}{\cos\beta} - 1\right]. \tag{4.33}$$

Since γ is smaller than β, but relatively close in size, the fraction, $\frac{\cos\gamma}{\cos\beta}$, can be approximated to equal 1, which allows the second term to go to zero. The error then scales as $\frac{1}{\cos\beta}$. Since the highest β value is 8° (previous results), the largest deviation between

these two equations will be at the level of $\sim 1\%$. The error is considered to be systematic due to $V_{H\alpha}$ not necessarily being along the same line as V_1, where the angle difference of β originates (Figure 4.3). Since the error caused by neglecting the impact of β is minimal compared to observational error, we can safely ignore it. Taking β to be 8° is the most extreme case. Depending on the projected separation or baseline length, which can be seen from Figure 4.5b, the Hα channel intersects the value of β at different values which will average out to be less than 8°.

Since β will not affect the visibilities to any great degree, equation 4.30 can be used to obtain the disk size and structure. As long as the c_p can be estimated, and $V_{binarymodel}$ properly obtained, the cancellation will leave the squared visibility of the disk alone with no other signal involved. For all the other channels (i.e. continuum channels that do not contain Hα emission) we would expect

$$V_{channel} = \sqrt{V^2_{binary}} - \sqrt{V^2_{binarymodel}} \approx 0. \tag{4.34}$$

which represents only the residuals and will help us assess how well the binary signature is being modeled and removed.

4.3 Disk Parameters

The method described in section 4.2 was implemented in an IDL program (besa.pro). Nights that had been processed in OYSTER were read into the program. The individual scans were fitted with a cosine function to get the $V^2_{\text{binarymodel}}$ and then, after the square root was taken, subtracted from the continuum channels and channel 10. Once each night was processed, they were combined into individual years and disk parameters were extracted from the data. In channel 10, which contains the disk parameters, the necessary parameter was c_p calculated using equation 4.24. The c_p values for different observing seasons are listed in Table 4.1.

If the binary signature is removed correctly from channel 10, the signature that remains is just the disk itself and no star or binary signature is present. The data points were very near zero for squared visibility. In the visibility context, the data was allowed to fluctuate around zero and allowed to be negative, but when the data was squared, it was biased toward the positive side. This ended up pulling the fitted Gaussian curve upward (Figure 4.6a). The solution chosen to correct for this bias was to insert a signature due to a synthetic star. Each synthetic star has a photospheric contribution c_p added to the contribution from the disk. It was found that each synthetic signature added to the signal in channel 10 made a difference in the derived disk size. The value used to determine the disk size was the photospheric contribution specifically calculated for the Hα channel.

This is because it should directly relate to how much the star is contributing to the signal. The range that was used to find the errors on the resulting disk size was a c_p of 0.5 to 0.9 for 2005 through 2009 (Figures 4.6b, 4.6c, and 4.6d for c_p values of 0.5, 0.8269, an 0.9 respectively) and 0.8 to 0.9 for 2010 and 2011. The reason the range for 2010 and 2011

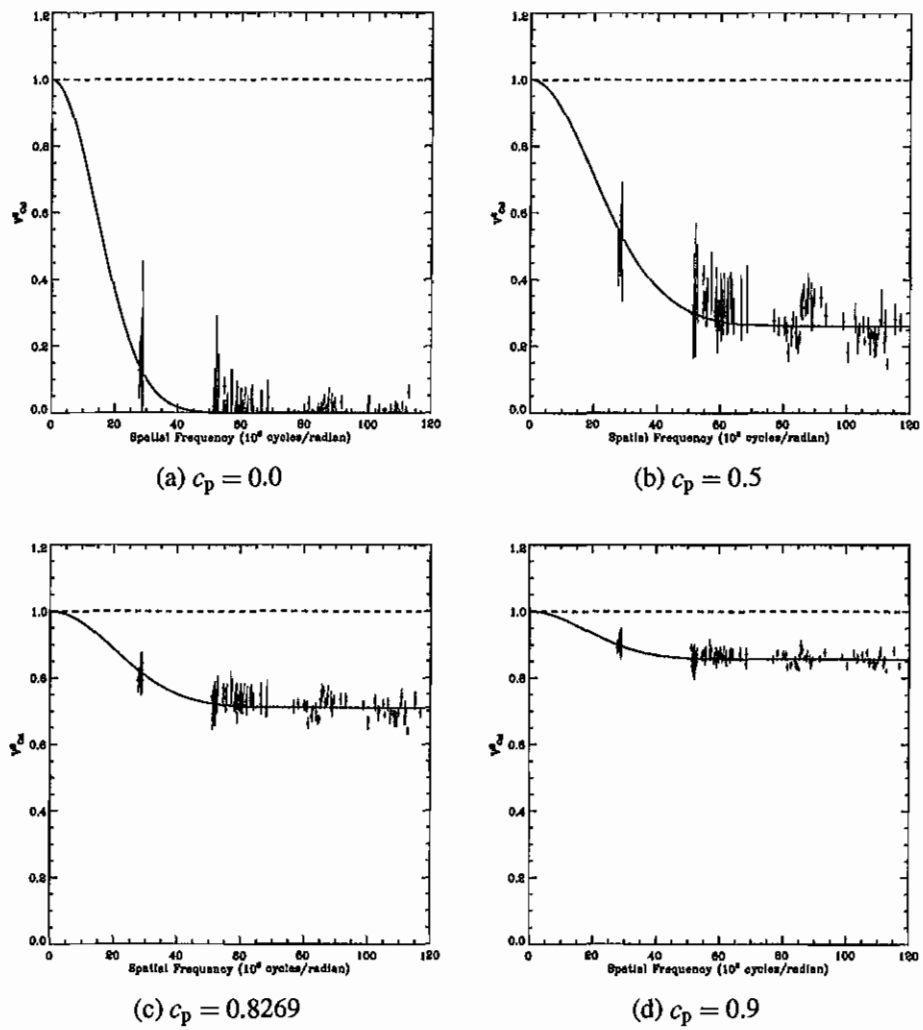

(a) $c_p = 0.0$ (b) $c_p = 0.5$

(c) $c_p = 0.8269$ (d) $c_p = 0.9$

Figure 4.6. Disk size fitted, to 2005 data, with a Gaussian. Each panel represents separate synthetic stars added to the data set with different c_p values. In this case, the most realistic synthetic star addition is the $c_p = 0.8269$ because that should be how much the star actually contributes to the system.

is smaller is because we are losing the disk (the equivalent width is decreasing for those seasons) and for any lower synthetic c_p values, the bias from the folding over would occur.

After each year was processed using the data from Table A.1, the disk size was determined (Table 4.2 results and Figure 4.7 for graphical representation). It can be seen that

Table 4.2. Disk size

Year	Disk size (mas)
2005	3.74 ± 0.42
2006	4.63 ± 0.26
2007	3.92 ± 0.22
2008	4.17 ± 0.26
2009	4.32 ± 0.93
2010	2.63 ± 0.42
2011	2.39 ± 0.21

the disk remained fairly stable up until 2010 and then it started to decrease in size (Figure 4.7). The decreasing disk size correlates with a decreasing equivalent width emission in Hα from the disk (Table 4.1).

Miroshnichenko et al. (2003) commented that the interaction with secondary stopped the disk from growing while the secondary was very close to the primary. The necessity for observing the system during the periastron passage interferometrically, for disk size, and spectroscopically, for temperature distribution and equivalent width measurements, is absolutely critical to determine how the disk growth occurs and fluctuates for a close binary system especially during the upcoming periastron passage in the summer of 2011.

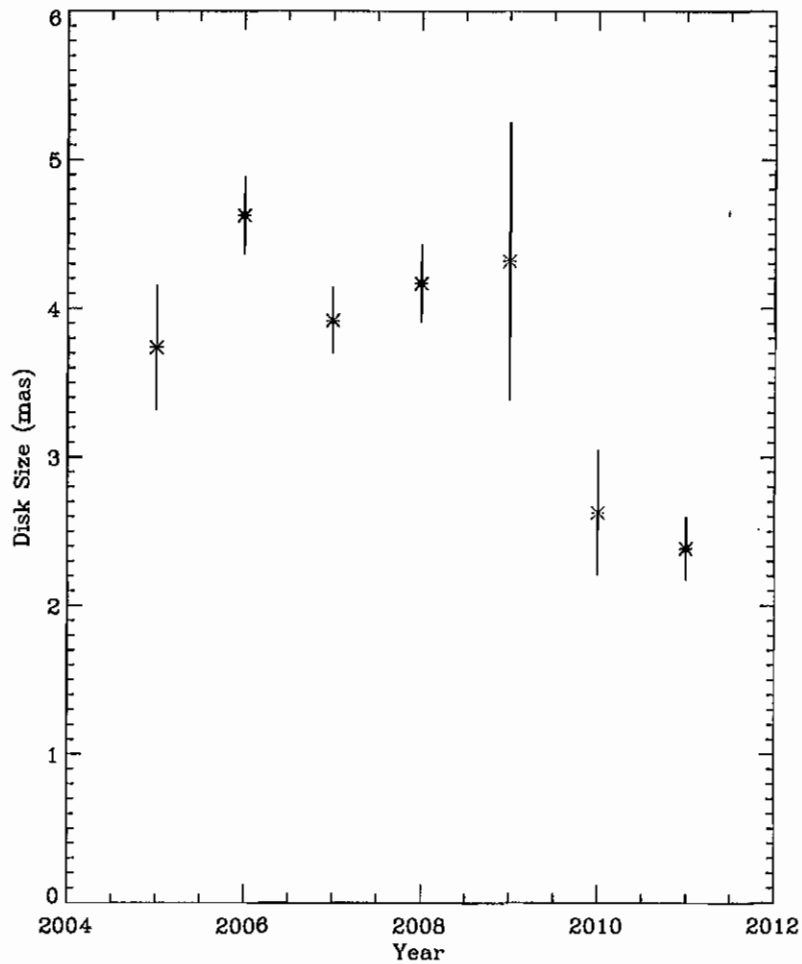

Figure 4.7. Disk size plotted as a function of time. The averaged values with the errors are from Table 4.2.

CHAPTER V

CONCLUSIONS

5.1 Binary Orbit

The campaign for revising the δ Sco binary system was one of the most important results for the astronomical community studying this system. Not only did the revision of the orbital parameters refine the shape and orientation of the orbit, it precisely predicted the periastron passage to within a few days. The orbit published in Tycner et al. (2011) has data up through 2010 and with the 2011 data set, the position and path the secondary is taking is confirming that the orbital parameters obtained as part of this study are an excellent representation of this binary system and will be able to guarantee that the periastron passage is going to be near July 5, 2011 $\pm$ 1 day.

A recent paper by Meilland et al. (2011) has confirmed with additional data from VLTI/AMBER and CHARA/VEGA, that the periastron date is July 5, 2011 $\pm$ 4 days. This result is within error of the Tycner et al. (2011) paper and this work's results. As the predicted periastron date approaches, many astronomers have already been collecting data and are waiting in anticipation for the chance to study the interaction between the secondary and primary star. This has been made possible through the precise revision of the orbital parameters and period of the binary.

5.2 CS Disk

Through the new method described in chapter IV, the size of the disk could be separated and extracted from the binary signature. It was necessary to add a synthetic signature due to a star to the data so that the bias that was caused by squaring the visibilities could be eliminated. This caused the size of the disk to change for a particular choice of contribution from a synthetic star, but resulted in a reasonable range of disk size. It can be seen from table 4.2 that disk maintained a relatively stable size from 2005 until 2009. The model fit to the disk indicated it was not a ring-like structure as thought in previous studies, but a uniform disk structure. As the secondary came closer to the primary star, the disk decreased in size. At the periastron passage, due to the minimum separation of $\rho_{min} = 6.04 \pm 0.07$ mas, there will be strong interaction between the secondary and CS disk.

Recent results from Meilland et al. (2011) disagree with these results in that they concluded that the disk did not grow or shrink during the observational period between 2007-2010. They do agree, however, that due to the relatively close separation between the two stars during the periastron passage, there will be significant interaction between the previously ejected matter and the secondary. Needless to say, observations during the periastron passage are vital to understanding the interaction of the disk and the secondary in a close binary system. This may provide insight into the mass transfer mechanism

associated with these types of systems as well as help enlighten how the disk formation occurs.

5.3 Future Work

To constrain all the orbital parameters, obtaining data for the following year (2012) would have enough of the orbit covered to give a definitive solution. The data points would be roughly at the same level as the 2010 data set but on the opposite side of the orbit. So not only would there be data from the periastron, but the data would be in all four quadrants of the orbit. Once the data is plotted and fit, the orbital parameters would be very well known.

Once the periastron data is obtained and reduced, it will give insight as to what interactions are occurring during that time period. That particular data set will show how the disk size is changing during the periastron passage which will enlighten how the secondary affects the disk and primary. Once 2012 data is obtained, it will show whether the disk does grow after the periastron which would be in agreement with the previous periastron passage (Miroshnichenko et al., 2001). At that point, modeling the temperature distribution and structure would also give a good indication as to how the secondary interacts and affects the disk. Once all of these data sets are obtained and reduced, it will a give good idea of how the δ Sco system operates and hopefully give some insight as to how circumstellar disks are formed in a interacting binary systems.

APPENDICES

APPENDIX A

ASTROMETRIC DATA

UT Date	JY	ρ	θ	Error Ellipse			σ_ρ	σ_θ	χ^2
				σ_{maj}	σ_{min}	ϕ			
	(yr)	(mas)	(deg)	(mas)	(mas)	(deg)	(mas)	(deg)	
2000 July 27	2000.5690	19.88	50.62	1.640	0.174	12.8	0.0642	0.1504	7.4
2000 July 28	2000.5718	20.20	49.37	1.348	0.159	8.5	0.0243	0.0592	95.1
2005 June 03[1]	2005.4205	189.84	352.76	5.024	0.151	9.1	0.7597	0.0725	35.6
2005 June 04[1]	2005.4232	189.86	352.75	0.691	0.147	9.9	0.0241	0.0029	105.9
2005 June 06[1]	2005.4287	189.87	352.75	0.651	0.153	11.0	0.0413	0.0049	143.7
2005 June 28	2005.4889	191.49	353.01	0.847	0.096	179.6	0.0342	0.0014	27.9
2005 June 29	2005.4917	191.39	352.99	0.804	0.086	175.3	0.0305	0.0012	13.2
2005 June 30	2005.4944	191.25	353.01	0.844	0.081	174.8	0.0176	0.0006	31.5
2005 July 01	2005.4971	190.98	353.01	0.778	0.091	178.4	0.0300	0.0012	12.1
2005 July 02	2005.4999	191.06	353.00	0.787	0.092	177.0	0.0325	0.0016	30.1
2005 July 03	2005.5026	191.41	353.04	0.870	0.087	175.4	0.0519	0.0018	19.4
2005 July 04	2005.5054	190.96	353.03	0.806	0.091	176.9	0.0479	0.0017	18.8
2005 July 05	2005.5081	191.26	353.04	0.870	0.083	177.4	0.0305	0.0014	11.3
2005 July 06	2005.5108	191.13	353.05	0.842	0.086	178.4	0.0157	0.0006	26.8
2005 July 09	2005.5191	191.51	353.08	0.860	0.083	177.4	0.0202	0.0008	38.2
2005 July 11	2005.5245	191.30	353.09	0.800	0.088	176.9	0.0269	0.0012	22.9

Continued on next page

UT Date	JY	ρ	θ	Error Ellipse			σ_ρ	σ_θ	χ^2
				σ_{maj}	σ_{min}	ϕ			
	(yr)	(mas)	(deg)	(mas)	(mas)	(deg)	(mas)	(deg)	
2005 July 12	2005.5273	191.50	353.11	0.833	0.084	177.2	0.0204	0.0008	20.0
2005 July 13	2005.5300	191.50	353.11	0.833	0.090	178.1	0.0303	0.0012	16.6
2006 April 12	2006.2774	191.53	354.97	0.449	0.088	3.5	0.0345	0.0020	32.7
2006 April 25	2006.3130	191.89	355.12	0.446	0.084	1.8	0.0241	0.0015	48.5
2006 April 30	2006.3267	191.88	355.17	0.816	0.296	144.2	0.0610	0.0139	71.5
2006 May 03	2006.3349	191.59	355.20	0.427	0.206	11.5	0.0210	0.0039	22.0
2006 May 05	2006.3404	191.49	355.20	0.408	0.208	8.1	0.0122	0.0021	66.2
2006 May 06	2006.3431	191.40	355.20	0.429	0.200	10.1	0.0108	0.0016	66.2
2006 May 09	2006.3514	191.63	355.22	0.430	0.203	11.2	0.0104	0.0017	66.8
2006 May 10	2006.3541	191.47	355.22	0.452	0.203	13.9	0.0173	0.0033	55.4
2006 May 11	2006.3568	191.50	355.23	0.431	0.203	9.0	0.0110	0.0017	56.1
2006 May 12	2006.3596	191.48	355.27	0.423	0.208	13.8	0.0260	0.0047	18.7
2006 May 13	2006.3623	191.61	355.26	0.423	0.208	10.0	0.0164	0.0024	23.1
2006 May 14	2006.3650	191.60	355.30	0.469	0.198	15.5	0.0196	0.0034	66.4
2006 May 15	2006.3678	191.67	355.32	0.812	0.234	38.3	0.0372	0.0091	9.5
2006 May 16	2006.3705	191.56	355.26	0.421	0.206	14.0	0.0267	0.0037	21.8
2006 May 17	2006.3733	191.50	355.27	0.419	0.202	7.9	0.0094	0.0015	21.6
2006 May 18	2006.3760	191.81	355.30	0.428	0.199	6.2	0.0110	0.0017	31.7

Continued on next page

UT Date	JY	ρ	θ	Error Ellipse			σ_ρ	σ_θ	χ^2
				σ_{maj}	σ_{min}	ϕ			
	(yr)	(mas)	(deg)	(mas)	(mas)	(deg)	(mas)	(deg)	
2006 May 19	2006.3787	191.64	355.28	0.423	0.201	6.7	0.0125	0.0019	73.5
2006 May 20	2006.3815	191.74	355.31	0.445	0.208	15.6	0.0316	0.0061	14.3
2006 May 21	2006.3842	191.61	355.28	0.493	0.213	22.3	0.0305	0.0059	30.1
2006 May 23	2006.3897	191.61	355.36	1.098	0.122	175.0	0.0264	0.0011	65.6
2006 May 24	2006.3924	191.94	355.39	1.000	0.168	176.4	0.0479	0.0021	66.8
2006 May 25[1]	2006.3952	191.81	355.22	0.994	0.114	172.6	0.0019	0.0001	9999.9
2006 May 26	2006.3979	191.57	355.37	0.929	0.147	173.6	0.0628	0.0034	12.5
2006 May 29[1]	2006.4061	190.87	355.42	0.989	0.120	172.9	0.0453	0.0019	118.5
2006 June 01	2006.4143	191.98	355.42	0.978	0.129	174.8	0.0494	0.0024	7.9
2006 June 02[1]	2006.4171	192.50	355.40	1.085	0.252	8.6	0.0379	0.0035	1501.5
2006 June 03	2006.4198	190.90	355.42	1.074	0.287	7.2	0.1097	0.0116	33.6
2006 June 04	2006.4225	191.16	355.38	1.069	0.279	5.3	0.1390	0.0135	8.5
2006 June 05	2006.4253	191.67	355.43	0.960	0.137	171.4	0.0910	0.0065	11.9
2007 May 04[1]	2007.3370	185.08	357.75	1.057	0.153	31.8	0.0836	0.0153	14.7
2007 May 08	2007.3479	184.83	357.81	1.020	0.152	30.4	0.0174	0.0039	17.0
2007 May 09	2007.3507	185.12	357.91	0.810	0.227	38.0	0.0146	0.0036	38.2
2007 May 10	2007.3534	184.84	357.82	0.989	0.154	30.2	0.0164	0.0035	25.7
2007 May 11	2007.3561	184.80	357.82	0.938	0.158	29.7	0.0184	0.0037	24.1

Continued on next page

UT Date	JY	ρ	θ	Error Ellipse			σ_ρ	σ_θ	χ^2
				σ_{maj}	σ_{min}	ϕ			
	(yr)	(mas)	(deg)	(mas)	(mas)	(deg)	(mas)	(deg)	
2007 May 12[1]	2007.3589	184.82	357.85	0.992	0.155	30.8	0.0183	0.0039	16.8
2007 May 13[1]	2007.3616	185.05	357.89	0.962	0.156	30.2	0.0201	0.0041	27.4
2007 May 15	2007.3671	184.63	357.83	0.973	0.156	30.1	0.0166	0.0035	35.1
2007 May 16	2007.3698	184.62	357.83	1.049	0.148	30.8	0.0168	0.0034	19.4
2007 May 17	2007.3726	184.83	357.93	1.214	0.158	34.1	0.0535	0.0128	9.9
2007 May 18	2007.3753	184.73	357.91	0.493	0.092	4.7	0.0266	0.0016	22.0
2007 May 25	2007.3945	185.12	358.02	0.446	0.092	1.6	0.0268	0.0012	20.6
2007 May 26	2007.3972	184.73	358.06	0.913	0.232	141.0	0.0509	0.0091	73.2
2007 May 27[1]	2007.4000	184.54	358.01	9.127	0.097	6.6	9.9999	60.6972	337.7
2007 May 28	2007.4027	185.02	357.87	2.464	0.207	128.7	0.0866	0.0160	25.4
2008 June 25	2008.4814	166.71	1.23	4.592	0.110	13.9	0.0785	0.0226	6.2
2008 June 27	2008.4869	166.51	1.31	0.620	0.167	12.8	0.0638	0.0145	5.2
2008 June 29	2008.4924	166.34	1.32	1.973	0.054	14.2	0.0367	0.0093	22.7
2008 July 03	2008.5033	166.23	1.38	0.707	0.135	9.1	0.0221	0.0029	18.8
2008 July 08	2008.5170	166.00	1.46	0.711	0.133	12.6	0.0355	0.0048	10.7
2009 March 08	2009.1823	148.15	4.00	0.486	0.261	177.5	0.0189	0.0015	10.6
2009 March 11[1]	2009.1905	147.93	4.02	0.505	0.084	179.4	0.0259	0.0017	12.5
2009 March 15[1]	2009.2015	147.40	4.09	0.645	0.152	8.2	0.0672	0.0144	61.4

Continued on next page

UT Date	JY	ρ	θ	Error Ellipse			σ_ρ	σ_θ	χ^2
				σ_{maj}	σ_{min}	ϕ			
	(yr)	(mas)	(deg)	(mas)	(mas)	(deg)	(mas)	(deg)	
2009 March 16[1]	2009.2042	147.46	4.09	0.756	0.122	7.1	0.0197	0.0031	15.5
2009 March 17	2009.2069	147.37	4.08	0.778	0.119	6.9	0.0200	0.0041	14.0
2009 March 18	2009.2097	147.30	4.09	0.753	0.124	6.2	0.0155	0.0023	9.1
2009 March 19	2009.2124	147.00	4.10	0.803	0.120	5.6	0.0180	0.0024	7.8
2009 July 07	2009.5136	137.50	5.54	0.405	0.206	6.6	0.0120	0.0028	58.2
2009 July 08	2009.5163	137.47	5.52	0.438	0.191	6.9	0.0141	0.0032	44.1
2009 July 09	2009.5191	137.29	5.56	0.466	0.214	21.7	0.0279	0.0071	36.2
2009 July 10	2009.5218	137.30	5.63	0.456	0.207	14.2	0.0180	0.0040	24.4
2009 July 13	2009.5300	137.03	5.68	0.434	0.201	11.5	0.0167	0.0040	27.9
2009 July 14	2009.5327	136.75	5.67	0.434	0.201	11.5	0.0159	0.0039	20.3
2009 July 15	2009.5355	136.85	5.70	0.413	0.209	7.2	0.0149	0.0032	14.0
2009 July 27	2009.5683	135.78	5.84	0.441	0.200	12.1	0.0129	0.0030	16.1
2010 April 15	2010.2856	104.10	10.63	0.560	0.266	0.0	0.0146	0.0028	18.6
2010 April 16[1]	2010.2884	105.38	10.57	1.077	0.077	176.9	0.0675	0.0089	90.2
2010 April 17[1]	2010.2911	103.73	10.65	0.497	0.081	176.7	0.0265	0.0053	10.8
2010 April 25	2010.3130	102.69	10.84	0.524	0.081	177.6	0.0093	0.0015	47.7
2010 April 26	2010.3158	102.44	10.86	0.522	0.083	177.9	0.0118	0.0018	38.5
2010 April 27	2010.3185	102.47	10.88	0.457	0.100	7.9	0.0239	0.0032	139.7

Continued on next page

UT Date	JY	ρ	θ	Error Ellipse			σ_ρ	σ_θ	χ^2
				σ_{maj}	σ_{min}	ϕ			
	(yr)	(mas)	(deg)	(mas)	(mas)	(deg)	(mas)	(deg)	
2010 May 01[1]	2010.3295	101.88	11.00	0.530	0.262	177.7	0.0130	0.0021	38.4
2010 May 03[1]	2010.3349	101.39	11.11	0.412	0.120	7.3	0.0366	0.0075	21.0
2010 May 05	2010.3404	100.96	11.11	0.512	0.085	179.8	0.0129	0.0020	68.5
2010 May 07	2010.3459	100.50	11.24	1.043	0.087	1.9	0.0735	0.0067	33.8
2010 May 08	2010.3486	100.75	11.16	0.561	0.267	180.0	0.0146	0.0023	29.2
2010 May 09	2010.3514	100.77	11.20	0.481	0.086	1.3	0.0098	0.0015	27.7
2010 May 12[1]	2010.3596	98.07	9.40	0.552	0.295	26.7	0.0020	0.0006	9999.9
2010 May 15	2010.3678	99.77	11.42	0.656	0.229	34.9	0.0345	0.0110	17.1
2010 May 16	2010.3705	99.69	11.39	0.741	0.123	7.5	0.0201	0.0036	12.4
2010 May 19	2010.3787	99.09	11.47	0.788	0.115	7.7	0.0215	0.0030	6.8
2010 May 20	2010.3815	99.15	11.49	0.704	0.125	6.9	0.0232	0.0045	5.3
2010 May 21[1]	2010.3842	98.81	11.52	0.713	0.133	12.4	0.0228	0.0040	15.1
2010 May 25	2010.3952	98.30	11.63	0.747	0.123	5.8	0.0122	0.0020	13.3
2010 May 26	2010.3979	98.27	11.63	0.786	0.119	5.0	0.0116	0.0022	18.4
2010 May 27	2010.4006	98.04	11.66	0.747	0.125	5.3	0.0169	0.0039	9.8
2010 May 28	2010.4034	98.00	11.68	0.760	0.133	9.4	0.0177	0.0033	8.0
2010 May 29	2010.4061	97.69	11.74	0.712	0.122	7.8	0.0136	0.0024	36.6
2010 May 30	2010.4089	97.61	11.73	0.780	0.122	6.5	0.0176	0.0033	9.2

Continued on next page

UT Date	JY	ρ	θ	Error Ellipse			σ_ρ	σ_θ	χ^2
				σ_{maj}	σ_{min}	ϕ			
	(yr)	(mas)	(deg)	(mas)	(mas)	(deg)	(mas)	(deg)	
2010 May 31	2010.4116	97.47	11.75	0.732	0.125	6.0	0.0119	0.0019	16.9
2010 June 02	2010.4171	97.02	11.78	0.740	0.129	8.7	0.0267	0.0048	9.8
2010 June 25	2010.4800	93.59	12.51	1.770	0.089	3.4	0.0423	0.0052	41.8
2010 June 26	2010.4828	93.98	12.46	1.240	0.103	1.9	0.0633	0.0086	92.5
2010 June 27	2010.4855	93.37	12.56	1.097	0.089	178.9	0.0248	0.0038	104.9
2010 June 28	2010.4883	95.33	12.41	1.251	0.101	1.8	0.0619	0.0067	121.8
2010 July 03	2010.5019	91.96	12.79	1.305	0.090	3.1	0.0369	0.0044	22.0
2010 July 04[1]	2010.5047	92.24	12.83	5.544	0.113	5.1	0.4707	0.0381	28.9
2010 July 05	2010.5074	92.35	12.76	1.112	0.088	1.2	0.0246	0.0031	27.3
2010 July 07	2010.5129	92.46	12.75	1.194	0.096	2.4	0.0287	0.0028	30.7
2010 August 12[1]	2010.6115	87.79	13.93	5.827	0.129	7.7	0.6055	0.0454	41.6
2010 August 14	2010.6169	85.75	14.10	1.023	0.164	4.2	0.2793	0.0309	26.7
2011 March 11	2011.1891	41.12	28.97	1.399	0.108	2.9	0.0423	0.0285	7.0
2011 March 13	2011.1946	40.56	29.47	1.376	0.113	4.7	0.0423	0.0389	12.8
2011 March 16	2011.2028	40.55	29.16	1.363	0.114	4.8	0.0476	0.0321	44.7
2011 March 28	2011.2357	36.76	31.25	1.076	0.279	3.2	0.1840	0.1432	1.5
2011 March 29	2011.2384	37.26	31.28	1.204	0.126	6.2	0.0790	0.0540	13.0
2011 March 30[1]	2011.2412	40.38	31.04	3.599	0.161	16.4	0.6672	0.2123	17.9

Continued on next page

UT Date	JY	ρ	θ	Error Ellipse			σ_ρ	σ_θ	χ^2
				σ_{maj}	σ_{min}	ϕ			
	(yr)	(mas)	(deg)	(mas)	(mas)	(deg)	(mas)	(deg)	
2011 April 01[1]	2011.2466	31.34	36.30	1.396	0.124	7.7	0.0998	0.1029	40.6
2011 April 02	2011.2494	36.20	31.95	1.411	0.120	6.0	0.0705	0.0554	13.1
2011 April 05	2011.2576	35.37	32.39	1.341	0.116	4.2	0.0302	0.0270	29.0
2011 April 06[1]	2011.2603	33.04	36.83	1.039	0.124	3.3	0.4001	0.3316	16.0
2011 April 12	2011.2768	32.38	34.92	1.399	0.122	6.9	0.0480	0.0477	56.5
2011 April 13	2011.2795	32.67	34.52	1.412	0.118	6.2	0.0535	0.0522	11.3
2011 April 15	2011.2850	31.29	35.78	1.396	0.123	5.5	0.0430	0.0491	11.0
2011 April 16	2011.2877	32.31	34.55	1.441	0.122	5.5	0.0532	0.0535	22.0
2011 April 17	2011.2904	30.61	36.47	1.350	0.116	4.1	0.0272	0.0330	14.4
2011 April 18	2011.2932	29.67	37.48	1.478	0.118	6.7	0.0460	0.0541	13.7
2011 April 21	2011.3014	28.49	38.75	1.412	0.121	5.4	0.0702	0.0929	19.0
2011 April 22	2011.3041	28.33	38.93	1.404	0.123	7.3	0.0417	0.0535	25.0
2011 April 25	2011.3123	28.08	38.97	1.334	0.127	7.4	0.0571	0.0758	12.8
2011 May 01	2011.3288	26.62	40.74	1.468	0.125	8.9	0.0909	0.1126	38.3
2011 May 02	2011.3315	25.69	41.53	1.368	0.123	5.2	0.0482	0.0753	29.3
2011 May 03	2011.3342	25.31	42.02	1.435	0.118	5.9	0.0408	0.0684	9.0
2011 May 04	2011.3370	25.17	42.26	1.369	0.122	5.6	0.0358	0.0613	8.1
2011 May 05	2011.3397	24.76	42.71	1.376	0.120	5.3	0.0271	0.0482	11.7

Continued on next page

UT Date	JY	ρ	θ	Error Ellipse			σ_ρ	σ_θ	χ^2
				σ_{maj}	σ_{min}	ϕ			
	(yr)	(mas)	(deg)	(mas)	(mas)	(deg)	(mas)	(deg)	
2011 May 15	2011.3671	21.44	47.43	1.264	0.117	6.6	0.0168	0.0393	30.3
2011 May 16	2011.3698	20.99	47.96	1.327	0.123	4.5	0.0611	0.1565	11.1
2011 May 22	2011.3863	19.53	49.79	1.328	0.117	4.3	0.0232	0.0698	11.2
2011 May 23	2011.3890	18.97	51.40	1.375	0.123	5.7	0.0470	0.1384	16.0
2011 May 24	2011.3917	18.85	51.31	1.369	0.122	5.6	0.0240	0.0757	25.8
2011 May 25	2011.3945	18.54	51.91	1.338	0.116	4.2	0.0158	0.0536	16.8
2011 May 27	2011.4000	18.48	51.29	1.219	0.137	9.6	0.0710	0.1886	28.7

Notes.

[1]Data removed from analysis.

APPENDIX B

RADIAL VELOCITIES

Date	Epoch JD	RV (k s^{-1})	RV Error
2000 July 28	2451754.286	-17.0	2.0
2000 August 04	2451761.575	-19.5	2.0
2000 August 07	2451764.246	-18.5	2.0
2000 August 07	2451764.568	-21.0	2.0
2000 August 09	2451766.258	-19.5	2.0
2000 August 10	2451767.592	-19.5	2.0
2000 August 12	2451769.269	-25.0	2.0
2000 August 20	2451777.225	-28.0	2.0
2000 August 20	2451777.546	-28.5	2.0
2000 August 24	2451781.577	-30.0	2.0
2000 August 30	2451787.566	-35.0	2.0
2000 August 31	2451788.548	-38.5	2.0
2000 September 04	2451792.538	-48.5	2.0
2000 September 06	2451794.541	-48.0	2.0
2000 September 12	2451800.527	-54.0	2.0
2000 September 13	2451801.525	-49.0	2.0
2000 September 16	2451804.532	-46.0	2.0
2000 September 17	2451805.524	-40.5	2.0
2000 September 18	2451806.508	-38.5	2.0
2000 September 19	2451807.506	-41.5	2.0
2000 September 21	2451809.506	-33.5	2.0
2000 September 26	2451814.494	-30.5	2.0
2000 September 27	2451815.502	-31.0	2.0
2000 September 28	2451816.503	-26.0	2.0
2000 October 03	2451821.497	-24.5	2.0
2000 October 23	2451841.493	-18.0	2.0
2001 February 10	2451951.948	-8.5	2.0
2001 February 20	2451961.904	-8.0	2.0
2001 February 27	2451968.978	-7.5	2.0
2001 March 10	2451978.944	-7.5	2.0

Notes.
Radial velocities from Miroshnichenko et al. (2001).

APPENDIX C

OYSTER FILES

C.1 double.model

```
; Global parameters:

starid ='FKV0594'

wavelengths =[0.800]

rv =-7.00 → addition to systematic RV is input here (Evans (1967) for δ Sco)

;

; Star parameters (for each star):

name(0) ='A'

code(0) =2

mass(0) =15.0 +/- 7.0 → Mass of the primary star (Tango et al. (2009) for δ Sco)

diameter(0) =1.2

teff(0) =0

logg(0) =0

magnitudes(*,0) =[0.0] → For Δm put the primary as zero

;

name(1) ='B'

code(1) =2

mass(1) =8.0 +/- 3.6 → Mass of the secondary star (Tango et al. (2009) for δ Sco)

diameter(1) =0.2

teff(1) =0

logg(1) =0
```

magnitudes(*,1) =[2.2] → Initial guess as to what the Δm will be

;

; Binary parameters (for each binary):

component(0) ='A-B'

method(0) =1 → If set for 1 then all binary parameters will be used as an initial guess. If set for 2 then only ρ and θ will be used as a guess

wdmode(0) =0

semimajoraxis(0)=104.0 → Initial guess (in mas)

eccentricity(0) =0.94 → Initial guess (Mason et al., 2009)

inclination(0) =39. → Initial guess (Mason et al., 2009)

periastron(0) =29.+180. → Initial guess (must add 180 degrees for convention (Mason et al., 2009))

ascendingnode(0)=153.0 → Initial guess (Mason et al., 2009)

period(0) =10.68*365.25 → Initial guess (years converted to days (Mason et al., 2009))

epoch(0) =2451797.6 → Oyster converts this to 11797.5 (i.e. Oyster shows

JD-2440000)

rho(0) =146.8

theta(0) =4.06

Orbital Fits to Data from Many Nights for Binary Systems

1. Create a single .psn file (make sure it has a .psn extension)

2. Read in the .psn file for binary positions use: → DATA → ASTROMETRY

3. To load in the Spectroscopic Data: → DATA → SPECTROSCOPY

   Note: make sure it has a .vel extension

4. To read the model type:

   - readmodel, 'double.model'
   - calcmodel
   - Note: make sure the "method" is set to "1" since that deals with binary parameters. "method 2" deals with calculating ρ and θ

5. Change the tolerance to 1E-10: → FIT → CONTROL

   - Note: this helps ensure that there will be no singular values

6. To fit for binary parameters and spectroscopic parameters use:

   → MODEL → FIT

   - Select the parameters you want to fit for:
     - Semi-major Axis (mas)
     - Eccentricity
     - Inclination Angle

- Periastron
- Ascending Node
- Period
- Epoch
- Mass for Primary "A"

- Start off with big steps (i.e. Lambda = 0.001) with a convergence of 0.0001. Once a local minimum is found, change Lambda to a sma ll step and continue to change as needed.

7. To make a plot for both astrometric data and spectroscopic data:

   → PLOT → ASTROMETRY

   → PLOT → SPECTROSCOPY

Fitting Binary Parameters to all V^2 Data

1. Read in all data by using: → DATA → INTERFEROMETRY

   Note: all .cha files must be in the same directory and Oyster must be run from that directory

2. Set the parallax using the command: set_parallax, 8.12, 0.88, 1

   Note: Each entry is: π, σ_π, and weight

3. If you want to solve for the Δm (both magnitudes for the stars), select Magnitude for the "B" component

4. To get a .psn file for all the data: → FIT → INTERFEROMETRY

APPENDIX D

IDL CODES

D.1 deltasco.pro

```
    PRO deltasco3

    COMPILE_OPT DEFINT32, STRICTARR, STRICTARRSUBS

    SET_PLOT, 'X' ; Select X-windows as a default display

    DEVICE, DECOMPOSED = 0 ; Colors are taken from a color table (not specified by R, G, B)

    LOADCT, 39, SILENT

    color_table = [60,250,150,220,30,90,110,190,10]

    color_text = ['blue','red','green', $

    'orange','violet','lt_blue','cyan','yellow','black']


psOutput = 1

    plotErrEllipse = 1

    pi = !DPI


;; binary parameters

    ;semi_major = 104.0 ;; Hartkopf (2009)

    ;i = 39.0 ;;inclination angle Hartkopf

    ;big_omega = 153.0 ;; Hartkopf

    ;ecc = 0.94 ;;eccentricity Hartkopf

    ;little_omega = 29 ;;Hartkopf

    semi_major = 99.1D ;; based on values from Christian
```

```
    i = 32.9D

    big_omega = 172.8D

    ecc = 0.938D

    little_omega = 2.1D

    period = 10.8170D

    T_epoch = 2000.6927D


;semi_major = 106.7 ;; Hartkopf (1996)

    ;i = 48.5 ;;inclination angle Hartkopf

    ;big_omega = 159.3 ;; Hartkopf

    ;ecc = 0.92 ;;eccentricity Hartkopf

    ;little_omega = 24 ;;Hartkopf

    ;semi_major = 98.3 ;; Sydney

    ;i = 38 ;;inclination angle Sydney

    ;big_omega = 175.2 ;; Sydney

    ;ecc = 0.9401 ;;eccentricity Sydney

    ;little_omega = 1.9 ;;Sydney

    ;semi_major = 107 ;; Miroshnichenko;

    ;i = 38 ;;inclination angle Miroshnichenko


       ;big_omega = 175 ;; Miroshnichenko

    ;ecc = 0.94 ;;eccentricity Miroshnichenko

    ;little_omega = -1 ;;Miroshnichenko
```

```
    ;; this sets the type of font to use on plots
    IF psOutput THEN dummyTitle='!6' ELSE dummyTitle='!3'
    WINDOW, 0, XSIZE=100, YSIZE=100
    PLOT, [0, 1], [0, 1], TITLE=dummyTitle
    WDELETE, 0


;; read in the synthetic data from the data.txt file
    ;data_file_name = 'noHa_98nights.txt' ;; note: this file has a longer lenght of first field
    data_file_name = 'noHa_96nights.txt' ;; note: this file has a longer lenght of first field
    ;; prepate the variables that will store the data
    epoch = DBLARR(200)
    rho = DBLARR(200)
    theta = DBLARR(200)
    majaxis = DBLARR(200)
    minaxis = DBLARR(200)
    PAerr = DBLARR(200)
    deltarho = DBLARR(200)
    deltatheta = DBLARR(200)
    chi2 = DBLARR(200)
    ;; check if the file exists
    checkFile = FILE_INFO(data_file_name)
    ;; if the file exists then read it in
    IF (checkFile.exists EQ 1) THEN BEGIN
```

```
tmp_1 = ''

tmp_2 = 0D

tmp_3 = 0D

tmp_4 = 0D

tmp_5 = 0D

tmp_6 = 0D

tmp_7 = 0D

tmp_8 = 0D

tmp_9 = 0D

tmp_10 = 0D

OPENR, file_unit, data_file_name, GET_LUN

counter = 0

WHILE NOT EOF(file_unit) DO BEGIN

;; read-in row by row

READF, file_unit, tmp_1, tmp_2, tmp_3, tmp_4, tmp_5, tmp_6, $

tmp_7, tmp_8, tmp_9, tmp_10, $

FORMAT='(A4, F11.4, F8.2, F8.2, F8.2, F6.3, F7.1, F9.4, F8.4, F7.1)'

;; assign the values from each row to the appropriate vector

epoch[counter] = tmp_2

rho[counter] = tmp_3

theta[counter] = tmp_4

majaxis[counter] = tmp_5

minaxis[counter] = tmp_6
```

```
    PAerr[counter] = tmp_7

    deltarho[counter] = tmp_8

    deltatheta[counter] = tmp_9

    chi2[counter] = tmp_10

        ;; adjust counter


    counter = counter + 1

    ENDWHILE

    CLOSE, file_unit

    FREE_LUN, file_unit

    ENDIF

    PRINT, 'Number of lines imported from ' + data_file_name $

    + ':  '  + STRING(counter)


;; strip the zeros

    epoch = epoch[0:counter-1]

    rho = rho[0:counter-1]

    theta = theta[0:counter-1]

    majaxis = majaxis[0:counter-1]

    minaxis = minaxis[0:counter-1]

    PAerr = PAerr[0:counter-1]

    deltarho = deltarho[0:counter-1]

    deltatheta = deltatheta[0:counter-1]
```

```
    chi2 = chi2[0:counter-1]


;; export the data back to an ascii format useful for latex paper
    julian_days = (epoch-2000.0)*365.25+2451545.0d0
    OPENW, text_file, 'table1.txt', /GET_LUN
    FOR j = 0, N_ELEMENTS(rho)-1 DO BEGIN
    ;; get the calendar date from JD
    CALDAT, julian_days[j], month, day, year
    PRINTF, text_file, STRING(FORMAT=
    '(I4, A4, I3, F10.4, F7.2, F7.2, F7.3, F7.3, F6.1)', $
    year, month2text(month), day, epoch[j],
    rho[j], theta[j], majaxis[j], minaxis[j], PAerr[j])
    ENDFOR
    CLOSE, text_file
    FREE_LUN, text_file


;; export IDL file with date and rho, theta
    CALDAT, julian_days, month_vec, day_vec, year_vec
    rho_vec = rho
    theta_vec = theta
    SAVE, FILENAME='delta-sco-rho-theta.dat',
    year_vec, month_vec, day_vec, rho_vec, theta_vec
```

```
;;converting rho and theta to cartesian coordinates

    phi = 90.0 - theta

    x = rho * cos(phi*(pi/180))

    y = rho * sin(phi*(pi/180))

    n = 10.0

    A = FINDGEN(n)/(n-1.0)*360*(!PI/180.0)

    USERSYM, COS(A), SIN(A), /FILL


;;make a circle representing the disk

    n3 = 1000.0

    B = FINDGEN(n3)/(n3-1.0)*360*(!PI/180.0)

    radius = 2.4/2.

    xcirc = radius * COS(B)

    ycirc = radius * SIN(B)

    IF psOutput THEN SET_PLOT, 'PS'

    ;IF psOutput THEN DEVICE, FILENAME='plot.ps', XSIZE=7, YSIZE=7, $

    XOFFSET=0.5, YOFFSET=3, ENCAPSULATED=0, /INCHES

    IF psOutput THEN DEVICE, FILENAME= 'plot_orbit.eps', XSIZE=6, YSIZE=7, $

    ENCAPSULATED=1, /INCHES

    ;IF psOutput THEN DEVICE, FILENAME='plot.eps', XSIZE=6, YSIZE=4,$

    ENCAPSULATED=1, /INCHES

    ;IF psOutput THEN DEVICE, FILENAME='plot.eps', ENCAPSULATED=1

    IF  psOutput THEN WINDOW, 0, XSIZE=800, YSIZE=1200
```

```
    IF psOutput THEN DEVICE, /COLOR, BITS_PER_PIXEL=8

    !P.POSITION = [0.1, 0.25, 0.9, 0.99]


;;plotting individual points

    PLOT, x, y, PSYM=8, SYMSIZE=0.5, THICK=7, XRANGE=[100.,-100.], YRANGE=[-10,210], $

    XSTYLE=1, YSTYLE=1, ISOTROPIC, CHARSIZE=0.7, CHARTHICK=2, $

    YTHICK=2, XTHICK=2, YTITLE='Declination Offset (mas)',$

    XTITLE='Right Ascension Offset (mas)';, TITLE='This Work'


;; overplot nice big ellipse

    yvaluese = ELLIPSE (-7.5,90.,102.5,31.5,-5.572, newxvaluese=xvaluese)

    ;OPLOT, xvaluese, yvaluese,LINESTYLE=1

    centerx=0

    centery=0

    OPLOT, [centerx], [centery], PSYM=7, THICK=1


;; overplot Tango et al. orbit

    ORBITS, 98.3, 38, 175.2, 0.9401, 1.9, 10.8, 2000.69, ECOORD=east, NCOORD=north,$

    XPER=x_per, YPER=y_per, TIMES=time

    OPLOT, east, north, color=color_table[3], THICK=1, LINESTYLE=2


;;overplot Miroshnichenko et al. orbit

    ORBITS, 107, 38, 175, 0.94, -1.0, 10.58, 2000.69, ECOORD=east, NCOORD=north,$
```

```
    XPER=x_per, YPER=y_per, TIMES=time
    OPLOT, east, north, color=color_table[2], THICK=1, LINESTYLE=4
    ;;overplot Mason et al. orbit
    ORBITS, 104, 39, 153, 0.94, 29.0, 10.68, 2000.69, ECOORD=east, NCOORD=north,$
    XPER=x_per, YPER=y_per, TIMES=time
    OPLOT, east, north, color=color_table[5], THICK=1, LINESTYLE=1

;; overplot the best-fit orbit
    ORBITS, semi_major, i, big_omega, ecc, little_omega, period, T_epoch, $
    ECOORD=east, NCOORD=north, XPER=x_per, YPER=y_per, TIMES=time
    OPLOT, east, north, color=color_table[0], THICK=2

index2 =WHERE(north EQ MIN(north))
    minimum_x = north[index2]
    minimum_y = east[index2]
    min_dist = SQRT((north)^2 + (east)^2)
    rho_min = MIN(min_dist)
    print, 'MIN SEP = ', rho_min
    shortest_dist_x = DBLARR(N_ELEMENTS(x))
    shortest_dist_y = DBLARR(N_ELEMENTS(x))
    shortest_time = DBLARR(N_ELEMENTS(x))

FOR j = 0, N_ELEMENTS(x)-1 DO BEGIN
```

```
yvaluese = ELLIPSE(x[j],y[j], majaxis[j], minaxis[j],PAerr[j],$
newxvaluese=xvaluese)
;; overplot small ellipse at each point
IF plotErrEllipse THEN OPLOT, xvaluese, yvaluese, LINESTYLE=0, $
color=color_table[1]
;;find the distance from the points to the ellipse using the time stamps

   hspace0.2indeltatime = epoch[j] - time shortest_time[j] = MIN(ABS(deltatime))
;;find which element in time vector is being used to calculate the
;;shortest time
index_short = WHERE(ABS(deltatime) eq shortest_time[j])
;; overplot an O-C vector
OPLOT, [x[j], east[index_short]], [y[j], north[index_short]], COLOR=color_table[0]
;; calculate the length of the O-C vector (x and y component separately)
shortest_dist_x[j] = x[j]-east[index_short]
shortest_dist_y[j] = y[j]-north[index_short]
ENDFOR


;;
;; PLOT #2 of 2
;; make a plot of the O-C values
;;
!P.POSITION = [0.1, 0.05, 0.90, 0.2]
```

```
theta_adjusted = theta

theta_adjusted[WHERE (theta GT 180.0)] = theta[WHERE(theta GT 180.0)] - 360.0

PLOT, theta_adjusted, shortest_dist_x, PSYM=6, XTITLE = 'P.A. (deg)',$

YTITLE='O-C (mas)', $

XSTYLE = 1, XRANGE = [-20, 60], $

CHARSIZE=0.7, CHARTHICK=2, YTHICK=2, XTHICK=2, SYMSIZE=0.7, YRANGE=[-2, 2],$

/NOERASE

OPLOT, theta_adjusted, shortest_dist_y, PSYM=7, SYMSIZE=0.7

OPLOT, [-180, 180], [0, 0], LINESTYLE=2

IF psOutput THEN DEVICE, CLOSE

SET_PLOT, 'X'

!P.POSITION = 0


;;

;; Make a separate plot of the periastron passage

;;

IF psOutput THEN SET_PLOT, 'PS'

IF psOutput THEN DEVICE, FILENAME= 'periastron_revised.eps', XSIZE=7, YSIZE=5.5,$

ENCAPSULATED=1, /INCHES

IF  psOutput THEN WINDOW, 1, XSIZE=900, YSIZE=800

IF psOutput THEN DEVICE, COLOR, BITS_PER_PIXEL=8

PLOT, x, y, PSYM=1, XTITLE='Right Ascension Offset (mas)',$

YTITLE='Declination Offset (mas)', XRANGE=[30.,-30.], YRANGE=[-20.,40.],$
```

```
    /ISOTROPIC, CHARSIZE=1, CHARTHICK=2, YTHICK=2, XTHICK=2, /NODATA
    OPLOT, [0], [0], PSYM=7, THICK=1
    OPLOT, east, north, color=color_table[0], THICK=2

;; find a point nearest to periastron
    index_peri = WHERE(ABS(time-T_epoch) EQ MIN(ABS(time-T_epoch)))
    OPLOT, east[index_peri], north[index_peri], PSYM=7, THICK=5

;; find points +/- 10 days from periastron

       day_offset = 10D
    OPLOT, east[WHERE(ABS(time-(T_epoch+day_offset/365.25)), $
    EQ MIN(ABS(time-(T_epoch+day_offset/365.25))))], $
    north[WHERE(ABS(time-(T_epoch+day_offset/365.25)), $
    EQ MIN(ABS(time-(T_epoch+day_offset/365.25))))], PSYM=5, THICK=5
    OPLOT, east[WHERE(ABS(time-(T_epoch-day_offset/365.25)), $
    EQ MIN(ABS(time-(T_epoch-day_offset/365.25))))], $
    north[WHERE(ABS(time-(T_epoch-day_offset/365.25)), $
    EQ MIN(ABS(time-(T_epoch-day_offset/365.25))))], PSYM=5, THICK=5

;; find points +/- 30 days from periastron
    day_offset = 30D
    OPLOT, east[WHERE(ABS(time-(T_epoch+day_offset/365.25)), $
```

```
    EQ MIN(ABS(time-(T_epoch+day_offset/365.25))))], $
    north[WHERE(ABS(time-(T_epoch+day_offset/365.25)),$
    EQ MIN(ABS(time-(T_epoch+day_offset/365.25))))], PSYM=4, THICK=5
    OPLOT, east[WHERE(ABS(time-(T_epoch-day_offset/365.25)), $
    EQ MIN(ABS(time-(T_epoch-day_offset/365.25))))], $
    north[WHERE(ABS(time-(T_epoch-day_offset/365.25)), $
    EQ MIN(ABS(time-(T_epoch-day_offset/365.25))))], PSYM=4, THICK=5

;; find points +/- 60 days from periastron
    day_offset = 60D
    OPLOT, east[WHERE(ABS(time-(T_epoch+day_offset/365.25)), $
    EQ MIN(ABS(time-(T_epoch+day_offset/365.25))))], $
    north[WHERE(ABS(time-(T_epoch+day_offset/365.25)), $
    EQ MIN(ABS(time-(T_epoch+day_offset/365.25))))], PSYM=6, THICK=5
    OPLOT, east[WHERE(ABS(time-(T_epoch-day_offset/365.25)), $
    EQ MIN(ABS(time-(T_epoch-day_offset/365.25))))], $
    north[WHERE(ABS(time-(T_epoch-day_offset/365.25)), $
    EQ MIN(ABS(time-(T_epoch-day_offset/365.25))))], PSYM=6, THICK=5

;; overplot the locations of the secondary based on the periastron
    ;; timings from Mirosh, Mason, and Tango
    ;; Mirosh
    custom_epoch = 2000.693 + 10.58D
```

```
    OPLOT, east[WHERE(ABS(time-custom_epoch) EQ MIN(ABS(time-custom_epoch)))], $
    north[WHERE(ABS(time-custom_epoch) EQ MIN(ABS(time-custom_epoch)))], $
    PSYM=1, THICK=5


;; Mason
    custom_epoch = 2000.693+ 10.68D
    OPLOT, east[WHERE(ABS(time-custom_epoch) EQ MIN(ABS(time-custom_epoch)))], $
    north[WHERE(ABS(time-custom_epoch) EQ MIN(ABS(time-custom_epoch)))], $
    PSYM=1, THICK=5


;; Tango
    custom_epoch = 2000.69389+ 10.74D
    OPLOT, east[WHERE(ABS(time-custom_epoch) EQ MIN(ABS(time-custom_epoch)))], $
    north[WHERE(ABS(time-custom_epoch) EQ MIN(ABS(time-custom_epoch)))], $
    PSYM=1, THICK=5


XYOUTS, [0],[-9.5], ['T!Do!N = 2011-07-06 !9+!X 2d'], CHARTHICK=1
    XYOUTS, [11,14,17],[6,15,28],['T!Do!N!E''''''!N (Tango et al.  2009)', $
    'T!Do!N!E''''!N (Mason et al.  2009)', $
    'T!Do!N!E''!N (Miroshnichenko et al.  2001)'] ,CHARTHICK=1, CHARSIZE=0.8
    IF psOutput THEN DEVICE, /CLOSE
    SET_PLOT, 'X'
    PRINT, 'End of main program.'
```

```
    END


FUNCTION ELLIPSE, x0,y0,maj,min,alpha, newxvaluese=xvaluese

    pi = !DPI

    n1 = 10000L


;;x range in the primed frame, where n is the size of the array and

    ;;'-100' is where it's shifted from, ie from -100 to 100

    x_prime = DINDGEN(n1)/DOUBLE(n1-1)*200-100


;;

    ;; select only positive values under the sqrt to avoid imaginary

    ;; numbers. Note: x model values need to be trimmed as well since

    ;; otherwise plotting x vs y will not work.

    ;;

    argument = 1.0 - ((x_prime)^2/min^2)

    index_pos_values = WHERE(argument GE 0.0)

    x_prime = x_prime[index_pos_values]

    sqrt_argument = argument[index_pos_values]

    y1eprime = maj*SQRT(sqrt_argument)

    y2eprime = -maj*SQRT(sqrt_argument)


;;rotation of the ellipse in the positive quadrants
```

```
    y1e = y1eprime * cos(alpha*(pi/180)) + x_prime * sin(alpha*(pi/180))

    x1e = x_prime * cos(alpha*(pi/180)) + y1eprime * sin(alpha*(pi/180))


;;rotation of the ellipse in the negative quadrants

    y2e = y2eprime * cos(alpha*(pi/180)) + x_prime * sin(alpha*(pi/180))

    x2e = x_prime * cos(alpha*(pi/180)) + y2eprime * sin(alpha*(pi/180))


;;adding a shift to the x and y values

    x1e = x1e + x0

    y1e = y1e + y0

    x2e = x2e + x0

    y2e = y2e + y0


;;reversing the coordinates so the ellipse will connect at the middle

    new_x2e = REVERSE(x2e)

    new_y2e = REVERSE(y2e)


;;returning both the xvalues and the y values as a vector

    xvaluese = [x1e, new_x2e, x1e[0]]

    RETURN, [y1e, new_y2e, y1e[0]]

    END
```

```
PRO orbits, a1, i , big_omega, ecc, little_omega, ECOORD=east, NCOORD=north, $
XPER=x_per, YPER=y_per, RTRUE=r_true, TIMES=time
pi = !DPI
;;In this case, the orbital values are read in from another
;;program. Usually it is read in through deltasco3.pro and returns the
;;values north, east, x_per, y_per, r_true, and time
;;In this case a1 is the semi-major axis, i is the inclination
;;angle, big_omega is the line of nodes, ecc is the eccentricity,
;;and little_omega is the relation of the true orbit to the line of nodes.
;;Each of these values are read in from another program.

;; converting all angles to radians
i = i*pi/180.
big_omega = big_omega*pi/180.
little_omega = little_omega*pi/180.

n = 100000
E = DINDGEN(n)/DOUBLE(n-1) * 4 * pi - 2 * pi ;;auxiliary angle (eccentric anomaly)
E_time = E*180.0/pi

;;the mean motion mu and period t in degrees/year and julian years respectively
P=10.81
```

```
    u = 360/P

    u_rad = (2*pi)/P

    T_epoch = 2000.6944D


;;x and y coordinates for the true orbit

    X = COS(E) - ecc

    Y = SQRT(1-(ecc^2)) * SIN(E)


;;Since there are two revolutions of the period there will no longer

    ;;be an exact number where E=0 since the numbers sampled will never be

    ;;enough to get E=0. Thus have to find the absolute value of the

    ;;smallest number that will be closest to 0 and still give the

    ;;relatively the same periastron passage distance within error.

    index_E = WHERE(ABS(E) eq MIN(ABS(E)))


;;finding the x and y coordinates of the true orbit when E=0.

    X_per_true = COS(E[index_E]) - ecc

    Y_per_true = SQRT(1-(ecc^2)) * SIN(E[index_E])


;;finding the r values of the true orbit.

    r_true = a1 * (1-ecc*COS(E))


;;finding the time vector corresponding the angle vector of E.
```

```
    time_num = E - ecc*SIN(E)

    time = time_num/u_rad + T_epoch


;;x and y coordinates multiplied by the semi-major axis

    xtrue = a1 * X

    ytrue = a1 * Y


;;Thiele-Innes constants for rectangular coordinates

    A = a1*(COS(little_omega)*COS(big_omega) -SIN(little_omega)*SIN(big_omega)*COS(i))

    B = a1*(COS(little_omega)*SIN(big_omega) +SIN(little_omega)*COS(big_omega)*COS(i))

    F = a1*(-SIN(little_omega)*COS(big_omega) -COS(little_omega)*SIN(big_omega)*COS(i))

    G = a1*(-SIN(little_omega)*SIN(big_omega) +COS(little_omega)*COS(big_omega)*COS(i))


;;relation between the true orbit and the apparent orbit

    x1 = A*X + F*Y

    y1 = B*X + G*Y


;;finding the first coordinates of the apparent orbit using the

    ;;index=0 since that corresponds to E=0 which is when the periastron occurs.

    x_per_sam = x1[0]

    y_per_sam = y1[0]


;;Again finding the periastron passage through a different method.
```

```
    x_per = A*X_per_true + F*Y_per_true

    y_per = B*X_per_true + G*Y_per_true


;;finding the radius (i.e. distance of the periastron passage) for

    ;;each individual case)

    ;;both rho_per1 and rho_per find the minimum rho in the true orbit

    ;;with finding E=0 in different methods.

    rho_per1 = SQRT((x_per_sam)^2 + (y_per_sam)^2)


;;this finds the radius of the true orbit

    rho_per = SQRT((x_per)^2 + (y_per)^2)


;;this finds the minimum distance for the apparent orbit

    rho_min = MIN(SQRT((x1)^2 + (y1)^2))

    north = x1

    east = y1

    END
```

```
    PRO errors
    SET_PLOT, 'X' ;Select X-windows as a default display
    DEVICE, DECOMPOSED = 0  ; Colors are taken from a color table (not specified by R, G, B)
    LOADCT, 39, /SILENT
    color_table = [60,250, 150,220,30,90,110,190,10]
    color_text = ['blue', 'red','green','orange','violet', $
    'lt_blue','cyan','yellow','black']


psOutput = 0
    pi = !DPI


;;sudo random number generator that is needed to start with a
    ;;seed. The same numbers are generated every time the program
    ;;is compiled.
    Seed = 24165L


;;sampled with 300,000 numbers
    n = 300000
     b = RANDOMN(Seed, n, /DOUBLE, /NORMAL)


;;the random numbers are generated around the mean value of all the
```

```
    ;;orbital parameters created in oyster. The standard deviation is the
    ;;errors also found in oyster.
    a = (b*0.047312826D) + 98.978779D
    incl = (b*0.2588893D) + 30.376811D
    big_omeg = (b*0.41893009D) + 172.28252D
    little_omeg = (b*0.48708858D) + 2.63476D
    e = (b*0.00069697829D) + 0.94126888D


rho_mins = DBLARR(n)
    rho_per = DBLARR(n)
    rho_true = DBLARR(n)
     IF psOutput THEN SET_PLOT, 'PS'

    ;IF psOutput THEN DEVICE, FILENAME='plot.ps', XSIZE=7, YSIZE=7,
    ;XOFFSET=0.5, YOFFSET=3, ENCAPSULATED=0, /INCHES
    IF psOutput THEN DEVICE, FILENAME='error.eps', XSIZE=7, YSIZE=7, XOFFSET=0.5, $
    YOFFSET=3, ENCAPSULATED=1, /INCHES
    ;ENCAPSULATED=1, /INCHES
    ;IF psOutput THEN DEVICE, FILENAME='plot.eps', ENCAPSULATED=1
    IF  psOutput THEN WINDOW, 0, XSIZE=600, YSIZE=600
    IF psOutput THEN DEVICE, /COLOR, BITS_PER_PIXEL=8


;;creating the size of the bins as well as the number of bins
```

```
no_of_bins = 50

my_bin_semi = (MAX(a)-MIN(a)) /DOUBLE(no_of_bins-1)

my_bin_incl = (MAX(incl)-MIN(incl)) /DOUBLE(no_of_bins-1)

my_bin_bomeg = (MAX(big_omeg) -MIN(big_omeg))/DOUBLE(no_of_bins-1)

my_bin_lomeg = (MAX(little_omeg) -MIN(little_omeg))/DOUBLE(no_of_bins-1)

my_bin_e = (MAX(e)-MIN(e)) /DOUBLE(no_of_bins-1)


;;creating the x-axis of bins centered at the mean value (how the bins

    ;;start are from the minimum value of the random variables)

    x_bins_semi = DINDGEN(no_of_bins) *my_bin_semi + MIN(a)

    x_bins_incl = DINDGEN(no_of _bins)*my_bin_incl + MIN(incl)

    x_bins_bomeg = DINDGEN(no_of _bins)*my_bin_bomeg + MIN(big_omeg)

    x_bins_lomeg = DINDGEN(no_of_bins) *my_bin_lomeg + MIN(little_omeg)

    x_bins_e = DINDGEN(no_of_bins) *my_bin_e + MIN(e)


;;the histograms of each of the orbital parameters created from the

    ;;number/size of the bins all should be centered at the mean value of

    ;;each randomly created numbers

    hist_semi = HISTOGRAM(a, NBINS=no_of_bins)

    hist_incl = HISTOGRAM(incl, NBINS=no_of_bins)

    hist_bomeg = HISTOGRAM(big_omeg, NBINS=no_of_bins)

    hist_lomeg = HISTOGRAM(little_omeg, NBINS=no_of_bins)

    hist_e = HISTOGRAM(e, NBINS=no_of_bins)
```

```
;;the bin centers are established. They have to be centered at the
    ;;bins and not on the edge due to both the Gaussian function and how
    ;;IDL plots the function so a half of a bin must be added to each x
    ;;value of the bin
    bin_centers_semi = x_bins_semi + 0.5*my_bin_semi
    bin_centers_incl = x_bins_incl + 0.5*my_bin_incl
    bin_centers_bomeg = x_bins_bomeg + 0.5*my_bin_bomeg
    bin_centers_lomeg = x_bins_lomeg + 0.5*my_bin_lomeg
    bin_centers_e = x_bins_e + 0.5*my_bin_e

;;the Gaussian using three parameters that give the standard
    ;;deviation, mean, and height
    nterms = 3
    x_gauss_semi = bin_centers_semi
    y_gauss_semi = GAUSSFIT(bin_centers _semi, hist_semi, coeff1, NTERMS=nterms)
    x_gauss_incl = bin_centers_incl
    y_gauss_incl = GAUSSFIT(bin_centers _incl, hist_incl, coeff2, NTERMS=nterms)
    x_gauss_bomeg = bin_centers_bomeg
    y_gauss_bomeg = GAUSSFIT(bin_centers _bomeg, hist_bomeg, coeff3, NTERMS=nterms)
    x_gauss_lomeg = bin_centers_lomeg
    y_gauss_lomeg = GAUSSFIT(bin_centers _lomeg, hist_lomeg, coeff4, NTERMS=nterms)
    x_gauss_e = bin_centers_e
```

```
    y_gauss_e = GAUSSFIT(bin _centers_e, hist_e, coeff, NTERMS=nterms)


;PLOT, bin_centers_semi, hist_semi, PSYM=10, TITLE='Histogram/Gaussian $
    of a', XTITLE='n=100000; MV=98.9786; !4r!X=0.047332098!COyster:  $
    MV=98.978779; !4r!X=0.047312826'
    ;PLOT, bin_centers_incl, hist_incl, PSYM=10,TITLE='Histogram/Gaussian &
    of !4i!X', XTITLE='n=100000; MV=30.37583; !4r!X=0.25899474!COyster:  &
    MV=30.376811; !4r!X=0.2588893'
    ;PLOT, bin_centers_bomeg, hist_bomeg, PSYM=10, TITLE='Histogram/Gaussian of !4X!X', $
    XTITLE='n=100000; MV=172.28093; $
    !4r!X=0.41910071!COyster:  MV=172.28252; !4r!X=0.41893009'
    ;PLOT, bin_centers_lomeg, hist_lomeg, PSYM=10, TITLE='Histogram/Gaussian$
    of !4x!X', XTITLE='n=100000; MV=2.6329045; !4r!X=0.48728696!COyster:  MV=2.63475; $
    !4r!X=0.48708858'
    ;PLOT, bin_centers_e, hist_e, PSYM=10, TITLE='Histogram/Gaussian of e', $
    XTITLE='n=100000; MV=0.94126624; !4r!X=0.00069726215!COyster:  $
    MV=0.94126888; !4r!X=0.00069697829'


;;attempting to find the minimum value of x and y (north and east
    ;;respectively) of each parameter while using random numbers with the
    ;;standard deviation and mean value found in oyster from our best fit
    ;;parameters. Once min of x and y are found, can find the min of rho
    ;;which will give errors on the periastron passage separation
```

```
FOR i=ULONG(0), N_ELEMENTS(a)-1 DO BEGIN

        semi_major = a[i] ;98.978779D ;a[i]


       inc = incl[i] ;30.376811D ;incl[i]

       big_omega = 172.28252D ;big_omeg[i]

       little_omega = little_omeg[i] ;2.63475D ;little_omeg[i]

       ecc = e[i] ;0.94126888D ;e[i]


   ORBITS, semi_major, inc, big_omega, ecc, little_omega, $

       ECOORD=east, NCOORD=north, XPER=x_per, YPER=y_per, RTRUE=r_true

        distances = SQRT((north)^2 + (east)^2)


       per_dist = SQRT((x_per)^2 + (y_per)^2)

        rho_mins[i] = MIN(distances)


       rho_per[i] = MIN(per_dist)

       rho_true[i] = MIN(r_true)

   ENDFOR


PRINT, MEAN(rho_mins)

   PRINT, MEAN(rho_true)

   PRINT, MEAN(rho_per)
```

```
;;calculating the minimum value of rho for the apparent orbit based on
    ;;the eccentric anomaly which is contained in the true orbit (also
    ;;when E = 0 then that is the time of the periastron passage
    no_of_bins_per = 60
    my_bin_per = (MAX(rho_per) -MIN(rho_per))/DOUBLE(no_of_bins_per-1)
    x_bins_per = DINDGEN(no_of _bins_per)*my_bin_per + MIN(rho_per)

hist_per = HISTOGRAM(rho_per, NBINS=no_of_bins_per)
    bin_centers_per = x_bins_per + 0.5*my_bin_per
    nterms1 = 3

    x_gauss_per = bin_centers_per
    y_gauss_per = GAUSSFIT(bin_centers_per, hist_per, coeff, NTERMS=nterms1)

print, coeff[0]
    print, coeff[1]
    print, coeff[2]
    PLOT, bin_centers _per, hist_per, PSYM=10,$

    TITLE='Histogram/Gaussian of !4q!X using all parameters as free parameters', $
    XTITLE='Mean value = 5.811747; !4r!X = 0.066997719!C Mean Value of !4q!X $
    apparent = 5.8098144; Mean Value r = 5.8132677'
    ;, SUBTITLE='Mean Value of !4q!X apparent = 5.8098389'
    OPLOT, x_gauss_per, y_gauss_per, THICK=2, COLOR= color_table[1]
```

```
;;calculating the minimum value of r for the true orbit based on
    ;;the eccentric anomaly which is contained in the true orbit (also
    ;;when E = 0 then that is the time of the periastron
    ;;passage). However, r min should give the periastron passage (closest
    ;;approach) in the true orbit. The value should correspond to rho_per
    ;;when E = 0.
    ;no_of_bins_r = 50
    ;my_bin_r = (MAX(rho_true) -MIN(rho_true))/DOUBLE(no_of_bins_r-1)

;x_bins_r = DINDGEN(no_of_bins _r)*my_bin_r + MIN(rho_true)
    ;hist_r = HISTOGRAM(rho_true, NBINS=no_of_bins_r)

    ;bin_centers_r = x_bins_r + 0.5*my_bin_r

    ;nterms3 = 3

    ;x_gauss_r = bin_centers_r
    ;y_gauss_r = GAUSSFIT(bin_centers_r, hist_r, coeff, NTERMS=nterms3)

;print, coeff[0]
    ;print, coeff[1]
    ;print, coeff[2]
```

```
;PLOT, bin_centers_r, hist_r, PSYM=10, TITLE= 'Histogram/Gaussian of r$
    using a as free parameter', XTITLE='Mean value = 5.8131351; !4r!X = $
    0.0027736385!CMean Value of !4q!X apparent = 5.8098389
    ;, SUBTITLE='Mean Value of !4q!X apparent = 5.8098389'
    ;OPLOT, x_gauss_r, y_gauss_r, THICK=2, COLOR=color_table[1]

;;calculating the minimum rho value of the apparent orbit using the
    ;north and east (x and y values) obtained from the whole orbit (using
    ;all of E). The minimum value should correspond to when E=0 in the
    ;apparent orbit. It will be smaller than the other two due to the
    ;apparent view on the sky (will appear to be closer than actually is)
    ;no_of_bins_rho = 50
    ;my_bin_rho = (MAX(rho_mins) -MIN(rho_mins))/DOUBLE(no_of_bins_rho-1)

;x_bins_rho = DINDGEN(no_of _bins_rho)*my_bin_rho + MIN(rho_mins)

;hist_rho = HISTOGRAM(rho_mins, NBINS=no_of_bins)

;bin_centers_rho = x_bins_rho + 0.5*my_bin_rho

;nterms2 = 3
    ;x_gauss_rho = bin_centers_rho
    ;y_gauss_rho = GAUSSFIT(bin_centers_rho, hist_rho, coeff, NTERMS=nterms2)
```

```
    ;print, coeff[0]

    ;print, coeff[1]

    ;print, coeff[2]


;PLOT, bin_centers_rho, hist_rho, PSYM=10, TITLE ='Histogram/Gaussian $

    of !4q!X using !4X!X as free parameter', XTITLE ='Mean value = 5.8098238; !4r!X = 0'

    ;OPLOT, x_gauss_rho, y_gauss_rho, THICK=2, COLOR=color_table[1]


IF psOutput THEN DEVICE, /CLOSE

    SET_PLOT, 'X'

    PRINT, 'End of main program.'


    END
```

```
    PRO binaryphase

    SET_PLOT, 'X'

    ; Select X-windows as a default display

    DEVICE, DECOMPOSED = 0

    ; Colors are taken from a color table (not specified by R, G, B)

    LOADCT, 39, /SILENT

    color_table = [60,250,150,220,30,90,110,190,10]

    color_text = ['blue','red','green', 'orange','violet','lt_blue', $

    'cyan','yellow', 'black']


psOutput = 1

    pi = !DPI

    n=100000


;wavelength used (850 nm - 550 nm) converted to meters

    lambda = DINDGEN(n)/DOUBLE(n-1)*350E-9+500E-9

    ;lambda = DINDGEN(n)/DOUBLE(n-1)*4000E-9+400E-9

    ;lambda = 656.281E-9 ;H alpha wavelength in meters

    lambda2 = lambda*1000000


;converting to microns

    B = 40.0D ; baseline vector, corresponds to length of the baseline in meters
```

```
;variable baseline length from 18 to 80 m

;B = DINDGEN(n)/DOUBLE(n-1)*62+18


;;spatial frequency (u,v) correspond to B_x and B_y

;;respectively. However in this case just using 1-D representation

f = B/lambda

;f2 = B2/lambda

;f3 = B3/lambda


;;converting the binary separation from mas to radians

rho = (192.92*pi)/(648000000)

rho2 = (20*pi)/(648000000)

rho3 = (100*pi)/(648000000)

;rho = (20*pi)/(648000000)

;rho = (DINDGEN(n)/DOUBLE(n-1)*192.92 + 86.42)*(pi)/(648000000)

;;projected binary separation along the baseline in radians

;p = DINDGEN(n)/DOUBLE(n-1)*rho

p = rho

p3 = rho2

p4 = rho3

p2 = (p*648000000)/pi ;converting back to mas


;;the angle that contains the dot product between the projected
```

```
    ;;separation and the spatial frequency
    psi = 2 * pi * p * f
    psi2 = 2 * pi * p3 * f
    psi3 = 2 * pi * p4 * f

;the delta m associated with the binary system
    ;deltam = 0.5D ;paper
    deltam = 2.2D ;Tango 2009
    deltam2 = 2.2D
    deltam3 = 2.2D

;intensity ratio associated of the components
    K = 10^(-deltam/2.5D)
    K2 = 10^(-deltam2/2.5D)
    K3 = 10^(-deltam3/2.5D)
    ;;angular diameter of the uniform disk for delta sco
    theta1 = (.45*pi)/(648000000)
    theta2 = (.2*pi)/(648000000)
    ;;for other stars from the paper
    ;theta1 = (1.0*pi)/(648000000)
    ;theta2 = (1.0*pi)/(648000000)

x_1 = (pi*theta1*B)/lambda
```

```
x_2 = (pi*theta2*B)/lambda

;;uniform disk diameter visibilities

v_1_top = BESELJ(x_1,1)

v_2_top = BESELJ(x_2,1)

v_1 = (2*v_1_top)/x_1

v_2 = (2*v_2_top)/x_2


;;the top and bottom portion of the phase deltam 2.2 and sep 192.92

phasetop = v_1 * SIN((K*psi)/(1+K)) - K * v_2 * SIN((psi)/(1+K))

phasebottom = v_1 * COS((K*psi)/(1+K)) + K * v_2 * COS((psi)/(1+K))


;deltam 1.0 or sep 20

phasetop2 = v_1 * SIN((K2*psi2) /(1+K2)) - K2 * v_2 * SIN((psi2)/(1+K2))

phasebottom2 = v_1 * COS((K2*psi2)/(1+K2)) + K2 * v_2 * COS((psi2)/(1+K2))


;deltam 3.0 or sep 100

phasetop3 = v_1 * SIN((K3*psi3)/(1+K3)) - K3 * v_2 * SIN((psi3)/(1+K3))

phasebottom3 = v_1 * COS((K3*psi3)/(1+K3)) + K3 * v_2 * COS((psi3)/(1+K3))


;deltam 2.2

phasetop_v1 = v_1*SIN((K*psi)/(1+K))

phasebottom_v1 = v_1* COS((K*psi)/(1+K))
```

```
;deltam 1.0

    phasetop_v12 = v_1*SIN((K2*psi2)/(1+K2))

    phasebottom_v12 = v_1* COS((K2*psi2)/(1+K2))


;deltam 3.0

    phasetop_v13 = v_1*SIN((K3*psi3)/(1+K3))

    phasebottom_v13 = v_1* COS((K3*psi3)/(1+K3))


phasetop_neg = (-phasetop)

    phasetop_neg1 =(-phasetop_v1)


;; the phase of the binary in radians

    ;; note: angle = ATAN(Y, X) if the result is supposed to be between -pi and pi

    phi = ATAN(phasetop, phasebottom)

    ;;converting back to degrees

    phi2 = (phi*180.)/pi


;deltam 1

    phi_1 = ATAN(phasetop2, phasebottom2)

    ;;converting back to degrees

    phi1 = (phi_1*180.)/pi


;;deltam 3
```

```
    phi_3 = ATAN(phasetop3, phasebottom3)
    ;;converting back to degrees
    phi3 = (phi_3*180.)/pi

;;phase of the binary in radians with a "negative" phase to see the
    ;;relation between phi and now phi3
    phi_neg = ATAN(phasetop_neg, phasebottom)
    phi_v1 = ATAN(phasetop_v1,phasebottom_v1)
    ;;converting back to degrees
    phi4 = (phi_neg*180.)/pi
    phi_4=(phi_v1*180.)/pi

;deltam 1
    ;phi3_32 = ATAN(-phasetop2, phasebottom2)
    phi_3_2 = ATAN(phasetop_v12,phasebottom_v12)
    ;;converting back to degrees
    ;phi42 = (phi3_32*180.)/pi
    phi_42=(phi_3_2*180.)/pi

;deltam 3
    ;phi3_33 = ATAN(-phasetop3, phasebottom3)
    phi_3_1_3 = ATAN(phasetop_v13,phasebottom_v13)
    ;;converting back to degrees
```

```
    ;phi43 = (phi3_33*180.)/pi

    phi_43=(phi_3_1_3*180.)/pi


;getting the remaining angle beta

    ;deltam 2.2

    beta = phi2-phi_4

    beta2 = phi1-phi_42

    beta3 = phi3-phi_43


;deltam 2.2

    index_low = WHERE(beta LT -320.0, count)

    index_high = WHERE(beta GT 320.0, count1)

    IF (count NE 0) THEN beta[index_low] = beta[index_low] + 360.0

    IF (count1 NE 0) THEN beta[index_high] = beta[index_high] - 360.0


;deltam 1

    index_low2 = WHERE(beta2 LT -320.0, count2)

    index_high2 = WHERE(beta2 GT 320.0, count22)

    IF (count2 NE 0) THEN beta2[index_low2] = beta2[index_low2] + 360.0

    IF (count22 NE 0) THEN beta2[index_high2] = beta2[index_high2] - 360.0


;deltam3

    index_low3 = WHERE(beta3 LT -320.0, count3)
```

```
    index_high3 = WHERE(beta3 GT 320.0, count33)
    IF (count3 NE 0) THEN beta3[index_low3] = beta3[index_low3] + 360.0
    IF (count33 NE 0) THEN beta3[index_high3] = beta3[index_high3] - 360.0

;;;;;;;;;;;;;;;;;;;;;;;;;;;;;;;;
    ;;Modulus of the visibility;;
    ;;;;;;;;;;;;;;;;;;;;;;;;;;;;;;;;
    modulusbottom = (1+K)^2
    modulustop1 = (K*v_2)^2 + (v_1)^2
    modulustop2 = 2*K*v_1*v_2*COS(psi)

vis_mod = (1/modulusbottom) *(modulustop1+modulustop2)
    vis_mod1 = SQRT(vis_mod)

im = vis_mod1 * SIN(phi)
    re = vis_mod1 * COS(phi)

IF psOutput THEN SET_PLOT, 'PS'
    ;IF psOutput THEN DEVICE, FILENAME='plot.ps', XSIZE=7, YSIZE=7,
    ;XOFFSET=0.5, YOFFSET=3, ENCAPSULATED=0, /INCHES
    IF psOutput THEN DEVICE, FILENAME='binaryphase.eps', XSIZE=7, YSIZE=7,$
    XOFFSET=0.5, YOFFSET=3, ENCAPSULATED=1, /INCHES
    ;IF psOutput THEN DEVICE, FILENAME='plot.eps', XSIZE=6, YSIZE=4,
```

```
    ;ENCAPSULATED=1, /INCHES
    ;IF psOutput THEN DEVICE, FILENAME='plot.eps', ENCAPSULATED=1
    IF  psOutput THEN WINDOW, 0, XSIZE=1200, YSIZE=800
    IF psOutput THEN DEVICE, /COLOR, BITS_PER_PIXEL=8

x = [0,1]
    y = [0,0]
    !P.MULTI = [0,1,3]

;plotting individual points
    PLOT, lambda2, beta2, THICK=1, XRANGE=[0.5,0.9],$
    CHARSIZE=1, $
    CHARTHICK=1, YTHICK=1,$
    XTHICK=1, YTITLE= 'Beta for 20 mas separation'
    ; PSYM=3;, YRANGE=[-15,15]
    ; TITLE='!7d!X Sco '

OPLOT, x, y, LINESTYLE=4
    OPLOT, [.656,.656],[-180,180], LINESTYLE=5
    ;OPLOT, [0,1], [0,0], LINESTYLE=4

PLOT, lambda2, beta3 , CHARSIZE=1, THICK=1, $
    XRANGE=[0.5, 0.9], YTITLE= 'Beta for 100 mas separation';, YRANGE=[-10,10]
```

```
    ;XTITLE='Wavelength, Baseline = 40 m, !7D!Xm = 2.2 !7q!X = 192.92 mas'
    OPLOT, [.656,.656],[-180,180], LINESTYLE=5
    OPLOT, x, y, LINESTYLE=4

PLOT, lambda2, beta, $
    XTITLE='Wavelength, Baseline = 40 m, !7D!Xm = 2.2',$
    YTITLE='Beta for 192.92 mas separation', XRANGE=[0.6, 0.9],$
    CHARSIZE=1;, YRANGE=[-10,10]
    OPLOT, [.656,.656],[-200,200], LINESTYLE=5
    OPLOT, x, y, LINESTYLE=4

;;plotting the real vs imaginary phase*visibility
    ;PLOT, re, im, PSYM=3, XTITLE ='Re (|V|cos!7u!X)', YTITLE='Im (|V|sin!7u!X)'

IF psOutput THEN DEVICE, /CLOSE
    SET_PLOT, 'X'
    PRINT, 'End of main program.'
    END
```

BIBLIOGRAPHY

Banerjee D. P. K., Janardhan, P., & Ashok, N. M. 2001, A&A, 380, L13

Bedding, T. R. 1993, AJ, 106, 768

A. F. Boden *Principles of Long Baseling Stellar Interferometry*, chapter 2, pp. 9–27, 1999 Michelson Summer School, Caltech, Pasadena, California, August 15–19, 1999.

Carciofi, A. C., Miroshnichenko, A. S., Kusakin, A. V., Bjorkman, J. E., Bjorkman, K. S., Marang, F., Kuratov, K. S., García-Lario, P., Calderón, J. V. P., Fabregat, J., & Magalhães, A. M., ApJ, 652, 1617

Collins, G. W., II, & Truax, R. J. 1995, ApJ, 439, 860

Cote, J., & van Kerkwijk, M. H. 1993, A&A, 274, 870

Cote, J., & Waters, L. B. F. M. 1987, A&A, 176, 93

Doazan, V., Sedmak, G., Barylak, M., Rusconi, L., & Battrick, B. 1991, ESA Special Publication, 1147

Evans, D. S. 1967, Determination of Radial Velocities and their Applications, 30, 57

Galazutdinov, G. A., & Krełowski, J. 2006, ApJ, 637, 342

Gandet, T. L., Otero, S., Fraser, B., & West, J. D. 2002, Information Bulletin on Variable Stars, 5352, 1

Gies, D. R. 2000, IAU Colloq. 175: The Be Phenomenon in Early-Type Stars, 214, 668

Herbert Goldstein, *Classical Mechanics, Second Edition*, Addison–Wesley Publishing Company, Reading, Massachusetts, USA, 1980.

Halonen, R. J., Jones, C. E., Sigut, T. A. A., Zavala, R. T., Tycner, C., Levine, S. E., Luginbuhl, C. B., Vlieg, N., & Vrba, F. J., PASP, 120, 498

Hanuschik, R. W., Hummel, W., Sutorius, E., Dietle, O., & Thimm, G. 1996, A&AS, 116, 309

Hartkopf, W. I., Mason, B. D., & McAlister, H. A. 1996, AJ, 111, 370

Wulff D. Heintz, *Double Stars*, D. Reidel Publishing Company, Boston, Massachusetts, USA, 1978.

Hummel, C. A., Benson, J. A., Hutter, D. J., Johnston, K. J., Mozurkewich, D., Armstrong, J. T., Hindsley, R. B., Gilbreath, G. C., Rickard, L. J., & White, N. M. 2003, AJ, 125, 2630

Innes, R. T. A. 1901, MNRAS, 61, 414

Jones, C. E., Tycner, C., & Smith, A. D. 2011, AJ, 141, 150

Koubský, P. 2005, Ap&SS, 296, 165

Mason, B. D., Hartkopf, W. I., Gies, D. R., Henry, T. J., & Helsel, J. W. 2009, AJ, 137, 3358

Meilland, A., Delaa, O., Stee, P., Kanaan, S., Millour, F., Mourard, D., Bonneau, D., Petrov, R., Nardetto, N., Marcotto, A., Clausse, J.-M., Perraut, K., Mcalister, H., Ten Brummelaar, T. A., Sturmann, J., Sturmann, L., Turner, N., Ridgway, S. T., Farrington, C., Goldfinger, P. J., & Farrington, C., arXiv:1106.1746

Millan-Gabet, R., Monnier, J. D., Touhami, Y., Gies, D., Hesselbach, E., Pedretti, E., Thureau, N., Zhao, M., ten Brummelaar, T., & the CHARA Group, ApJ, 723, 544

Miroshnichenko, A. S., Bjorkman, K. S., Morrison, N. D., Wisniewski, J. P., Manset, N., Levato, H., Grosso, M., Pollmann, E., Buil, C., & Knauth, D. C., A&A, 408, 305

Miroshnichenko, A. S., Fabregat, J., Bjorkman, K. S., Knauth, D. C., Morrison, N. D., Tarasov, A. E., Reig, P., Negueruela, I. & Blay, P., A&A, 377, 485

Mourard, D., Bonneau, D., Biazit, A., Labeyrie, A., Morand, F., Percheron, I., Tallon-Bosc, I., & Vakili, F. 1992, IAU Colloq. 135: Complementary Approaches to Double and Multiple Star Research, 32, 510

Otero, S., Fraser, B., & Lloyd, C. 2001, Information Bulletin on Variable Stars, 5026, 1

Porter, J. M., & Rivinius, T. 2003, PASP, 115, 1153

Porter, J. M. 1996, MNRAS, 280, L31

Silaj, J., Jones, C. E., Tycner, C., Sigut, T. A. A., & Smith, A. D. 2010, ApJS, 187, 228

Tango, W. J., Davis, J., Jacob, A. P., Mendez, A., North, J. R., O'Byrne, J. W., Seneta, E. B., & Tuthill, P. G. 2009, MNRAS, 396, 842

Tycner, C., Ames, A., Zavala, R. T., Hummel, C. A., Benson, J. A., & Hutter, D. J. 2011, ApJL, 729, L5

Tycner, C., Hajian, A. R., Armstrong, J. T., Benson, J. A., Gilbreath, G. C., Hutter, D. J., Lester, J. B., Mozurkewich, D., & Pauls, T. A., AJ, 127, 1194

Tycner, C., Lester, J. B., Hajian, A. R., Armstrong, J. T., Benson, J. A., Gilbreath, G. C., Hutter, D. J., Pauls, T. A., & White, N. M., ApJ, 624, 359

Waters, L. B. F. M. 1986, A&A, 162, 121